Large Eddy Simulations of Entrainment and Inversion Structure

Alison M. Fowler

Submitted in accordance with the requirements for the degree of
MRes: Physics of the Earth and Atmosphere

The University of Leeds
School of Earth and Environment

August, 2006

The candidate confirms that the work submitted is her own and that appropriate credit has been given where reference has been made to the work of others.

Acknowledgements

The author would like to acknowledge Dr I. Brooks who supervised this project and gave invaluable advice for its direction.

This research has been funded by the Natural Environment Research Council (NERC).

Abstract

This study has come about from the increasing research into the entrainment zone, but the lack of discussion of the key definitions used in its parameterizations. Using large eddy simulations a variety of entrainment zone definitions, currently in use, are focused on and their key advantages and disadvantages over one another are scrutinized. It is found that estimating the entrainment zone using area-averaged properties produces an incomplete picture, since those methods average out inherently small-scale and sporadic processes, and are inconsistent with the turbulent nature of the planetary boundary layer. However, defining the entrainment zone using a wavelet algorithm developed by Brooks (2003) proved to have a robust relationship with the convective Richardson number and also had the advantage of providing local estimates of the top and bottom of the entrainment zone. This has allowed the new study of the statistics of the distribution of the entrainment zones limits to be carried out, which proved to have an interesting correlation with the convective Richardson number. This relationship may now make it possible to parameterize the entrainment velocity in terms of the entrainment zone statistics.

The statistical properties of the mixed layer top, and in particular its distribution of 'upwellings' have also been studied. Leading to a new insight into the time and spatial scales involved in entrainment and how entrainment varies with the convective Richardson number. The decrease in time scale of an entrainment event as the Richardson number decreases is thought to be due to the decrease in the equivalent amount of energy needed for entrainment to occur.

Contents

Acknowledgements **2**

Abstract **3**

Contents **4**

Part 1 ..... **5**

1. INTRODUCTION 5

1.1 Objectives 6

2. DEFINITIONS OF ENTRAINMENT ZONE 7

2.1 Area of negative buoyancy flux 8

2.2 Probability distribution of the maximum gradient in a conserved scalar quantity 10

2.3 Significant gradient in a conserved scalar quantity 11

2.4 Wavelet algorithm 12

3. THE LARGE EDDY SIMULATION EXPERIMENTS 14

4. DESCRIPTION OF ENTRAINMENT EVENTS 17

4.1 Convective Richardson Number, Ri_* 17

4.2 The current understanding of entrainment events 18

4.3 Statistics of upwellings at the ML top 20

5. PARAMETERISATIONS 26

5.1 Entrainment Zone depth 26

5.2 Wavelet statistics of the entrainment zone 30

5.3 Entrainment velocity, w_e. 35

6. DISCUSSION AND CONCLUSIONS 38

7. REFERENCES 41

Part 2 Tables **44**

2.1. Tables 44

Part 3 Appendixes **45**

Appendix A: Abbreviations 45

Appendix B: Sensitivity Tests 47

Appendix C: The Shallow Mixed Layer 50

Appendix D: Literature Review 54

Part 1

1. INTRODUCTION

The entrainment zone (EZ) is the region at the top of the planetary boundary layer (PBL) where rising thermals overshoot upward of the mixed layer (ML) and warmer free troposphere air above is mixed downward into the ML. Figure 1.1. shows how the overshooting thermals distort the ML top. The rising thermals in the ML, which are positively buoyant at the surface due to surface heating, rise through the mixed layer until they reach the warmer free atmosphere and become negatively buoyant; they overshoot a small distance into the free atmosphere because of their momentum (Stull, 1988). This negatively buoyant air then sinks back down into the mixed layer intact, due to low turbulence in the free atmosphere, so pollutants from within the mixed layer stay within it. In the process of the thermals overshooting into the free atmosphere, free atmospheric air is drawn into the mixed layer and is quickly mixed in due to the strong turbulence within the mixed layer- thus the mixed layer grows. This makes entrainment important as it is responsible for the growth of the PBL which is an essential factor in the dilution and transportation of the pollutants emitted from the surface and also the turbulent structures within the PBL under unstable conditions, due to the height of the PBL limiting the vertical growth of the eddies (Gryning et al., 1987). Entrainment also plays a key role in determining the distribution and structure of the stratiform clouds, particularly marine stratocumulus which is an important factor affecting the global radiation budget, and hence climate. Entrainment affects the distribution of the cloud as the EZ top is a measure of the maximum height a rising thermal reaches. If the rising thermal reaches the lifting condensation level (LCL), then this may become a site of possible cloud formation. If the EZ is higher than the LCL then a stratocumulus deck can occur (Nelson et al. 1989). For these various reasons, it is desirable to be able to forecast entrainment parameters, such as depth and velocity.

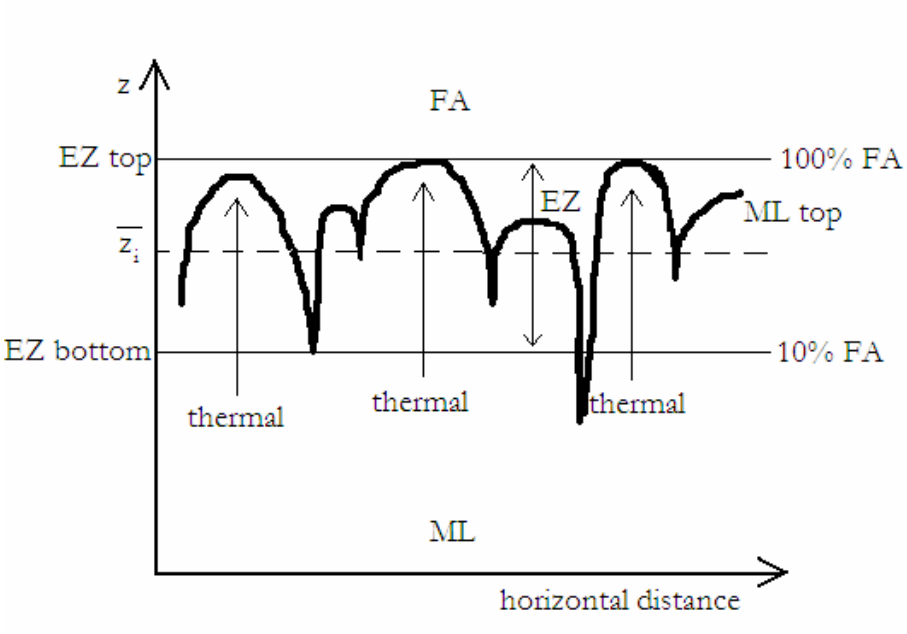

Figure 1.1. EZ defined in terms of the fraction of FA air. The solid line is the ML top, while the dashed line is the average ML top, $\overline{z_i}$ (Stull, 1988).

1.1 Objectives

Turbulence leading to entrainment can be caused by surface sensible and latent heating, cloud top radiative or evaporative cooling, wind shear or a combination (Lewellen and Lewellen, 1998). The following study uses a Large Eddy Simulation (LES) model to reproduce a convective cloud free boundary layer, in order to produce i) a critical review of current definitions of the EZ and ii) Create a new parameterization of the entrainment velocity.

2. DEFINITIONS OF ENTRAINMENT ZONE

The entrainment rate, w_e, is impossible to measure directly, so must be inferred from other measurements. It is commonly assumed the depth of the EZ relates directly to the entrainment rate, thus determining a measure of the entrainment zone depth becomes important for understanding entrainment.

$$\frac{w_e}{w_*} \propto \frac{\Delta h}{\overline{z_i}}, \qquad 2.i.$$

where w_* is the convective velocity scale, or Deardorff velocity, $\left[\frac{g z_i}{\overline{\theta}}\left(\overline{w'\theta'}\right)_s\right]^{1/3}$ (g is gravity, $\overline{\theta}$ is the mean potential temperature across the inversion and $\left(\overline{w'\theta'}\right)_s$ is the heat flux at the surface), Δh is the EZ depth and $\overline{z_i}$ is mean ML height. When there is little wind the entrainment velocity can be defined as:

$$w_e = \frac{\partial z_i}{\partial t} - w_L, \qquad 2.ii.$$

where w_L is the large-scale mean vertical velocity (negative for subsidence).

There has been much discussion over the exact form this relationship, 2.i., takes, ranging from a ¼ power relationship (Deardorff, 1983), a ½ power relationship (Boers, 1989), to a directly proportional relationship (Deardorff, 1980). Figure 2.1 shows that for the range of conditions used in this computational study, there is a linear relationship between the entrainment velocity and EZ depth. This predicts that when the entrainment velocity is zero, and there is no entrainment, the EZ depth will still be positive. This depends very much on the definition of EZ used; a lot of definitions do not go to zero largely because they are measuring something affected by factors other than entrainment. However, during day-time convective conditions it is true that the EZ should always exist.

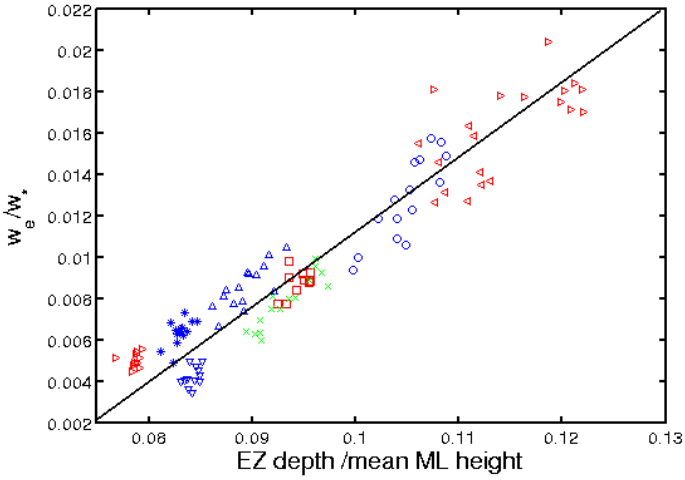

Figure 2.1. Entrainment velocity, w_e, normalised by the convection velocity scale, w_*, plotted as a function of EZ depth divided by mean ML height. The EZ depth has been estimated using the wavelet algorithm and the mean ML height comes from the average altitude of the maximum in the gradient of the water mixing ratio, q. For symbol definitions see Figure 4.1.1

The EZ top is defined as the maximum height of a rising thermal, the bottom is less well defined and is often understood to be the height where 90 to 95% of the air on a horizontal average has ML rather than free atmosphere, FA, characteristics (for example, in terms of turbulence, humidity or potential temperature) (Nelson et al. 1989), Figure 1.1. However, in terms of making measurements, in observational, laboratory and computational experiments, the entrainment zone has been defined in various ways which do not necessarily produce the same result or represent the same physical mechanisms; currently there is no universally applicable definition of the EZ. A summary of frequently used definitions follow.

2.1 Area of negative buoyancy flux

The area of negative buoyancy flux, $\overline{w'\theta'}$, in the inversion layer is often used as an indicator of net entrainment, as it defines the region of overshooting thermals into the warm FA which cause entrainment. A negative buoyancy flux signifies the consumption of turbulent energy as less dense air is mixed down into the boundary layer. The minimum value of the buoyancy heat flux is related explicitly to the growth of the BL by:

$$-\left(\overline{w'\theta'}\right)_{\min} = \Delta\theta \frac{dz_i}{dt}, \text{ (Tennekes and Driedonks, 1981)} \qquad 2.1.i$$

where $\Delta\theta$ is the change in potential temperature across the inversion.

This implies that $(\overline{w'\theta'})_{\min}$ is always negative as the inversion must be stable ($\Delta\theta$>0).

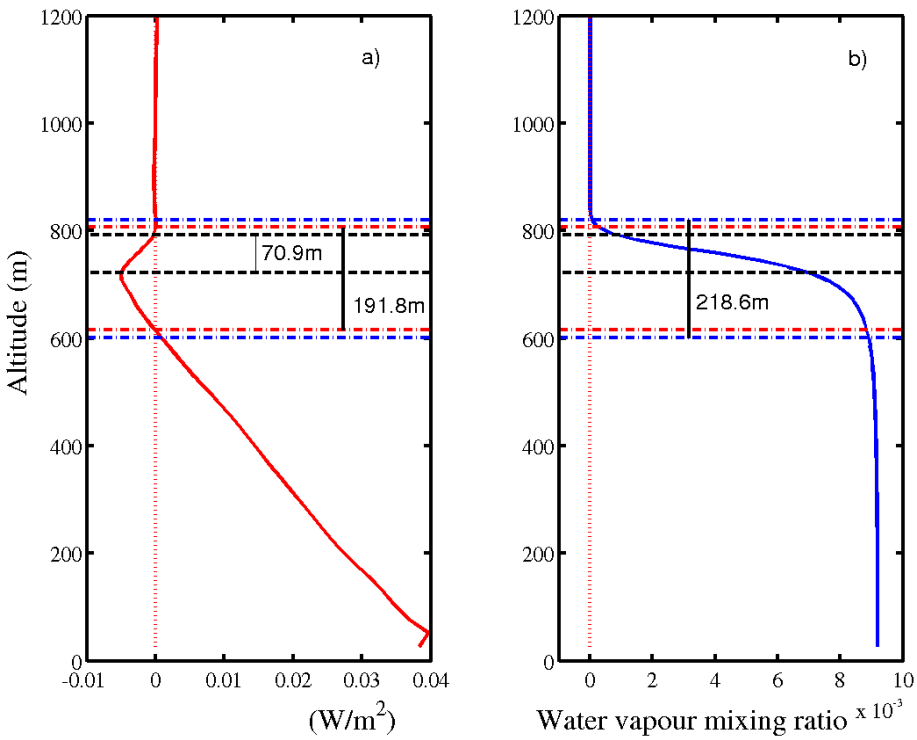

Figure 2.1.1. Comparing area averaged values for EZ top and EZ bottom. (**---** 95% and 5% limits of the variability in boundary layer top, defined by the maximum gradient in some conserved scalar (**-.-.**) area of negative buoyancy flux (**-.-.**) area of significant gradient in some conserved scalar). These are compared with a) the buoyancy flux profile and b) the profile for the water mixing ratio, q.

Figure 2.1.1a shows a typical area-averaged profile of the buoyancy flux (the red line) and the EZ depth it describes (red dot-dash line), which corresponds to the negative region. In some cases instead of the buoyancy flux reaching a maximum negative value then smoothly returning to a zero value where it will stay throughout the height of the FA, it may dip back to positive values first before settling at zero or may never fully settle at zero and fluctuate a small amount around zero high into the FA. For this reason, instead of defining the EZ top as the point where the buoyancy flux first becomes zero after

reaching its maximum negative value it is assumed here that the negative part of the profile is symmetrical and taken the EZ top to be twice the distance of the difference between the first negative value of the buoyancy flux (EZ bottom) and its maximum negative value (ML height) from the EZ bottom, which gives a less ambiguous definition of EZ top (see Figure 2.1.2).

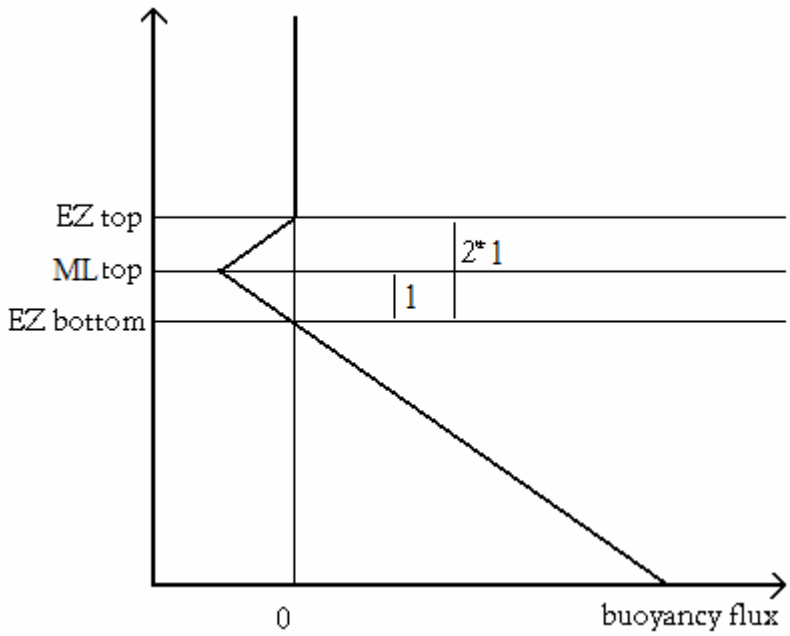

Figure 2.1.2. A schematic diagram of a typical buoyancy flux profile. 2*l=EZ depth.

Although this is the most physically meaningful estimate of the EZ, it is impossible to measure in-situ. So, in this study, it is of interest to find a relation between this definition and a definition which it is readily possible to make observations of.

2.2 Probability distribution of the maximum gradient in a conserved scalar quantity

This definition can be applied to lidar (LIght Detection And Ranging) backscatter signals of aerosols, which are in high concentration within the PBL but usually much lower above the inversion. The EZ, in observations, corresponds closely to the area where the concentration becomes diluted by FA air, and thus backscatter changes from PBL to tropospheric values. Although this is often assumed to occur in unison with the temperature inversion, it does not respond directly to the thermodynamic properties of the atmosphere.

In the large eddy model, this definition is applied to the profile of a conserved scalar quantity, by measuring the boundary layer height, taken as the height of the maximum gradient in the profile, at every single point in the domain. Then either the 1% and 99%, or the 5% and 95%, values of its probability distribution are taken to be the EZ bottom and EZ top respectively. In this study the 5-95% values will be used. Although this is a measure of the variability of the ML top rather than the EZ thickness, Davies et al. (1997), found the thickness of the EZ and the variability of the ML top to be highly correlated. In these simulations a measure of the water mixing ratio, q, is used as the conserved scalar quantity and assumed to behave in a similar way to lidar measurements of aerosol backscatter. However it is possible that backscatter from aerosols may also be affected by a change in relative humidity across the inversion layer (see section 3).

2.3 Significant gradient in a conserved scalar quantity

This definition is similar to the previous estimation, in that it uses a profile of some conserved scalar quantity. This time the EZ is estimated as the area where the mean gradient of this scalar quantity is thought to be significant. However, this may potentially lead to problems as the choice of significant gradient is somewhat arbitrary. In Figure 2.1.1b it is clear from a profile of the area average conserved scalar quantity that the EZ top is fairly well defined but the EZ bottom is less so, as the transition from EZ values to ML values is much more gradual, and many different points could be argued to be the EZ bottom.

In this study the significant gradient is taken to be the area where the gradient is greater than 1% of the maximum gradient. However, as the model warms up the profile may become less smooth and large gradients can also be found below the actual inversion which may lead to an estimate of the EZ depth which is too large, and does not accurately reflect the entrainment process which is occurring. Large background gradients have also been observed in the atmosphere especially under stable stratification where the inversion is deep and sometimes ill-defined.

2.4 Wavelet algorithm

Estimations which equate the area of negative buoyancy flux, or the area of significant gradient in a conserved scalar quantity to the EZ depth, both treat the EZ as a horizontally averaged property of the PBL top. However, Lilly (2002) noted that although the interface is usually quite abrupt locally horizontally averaged properties exhibit a more gradual change due to fluctuations of the interface height. These area averaged values of the EZ depth can be affected, for example, by gravity waves which vary the PBL depth without contributing to the inversion structure. Gravity waves depend on the static stability at the top of the ML; they can propagate vertically or horizontally away from the thermals using only a small amount of the thermals' momentum and kinetic energy. It may be possible to filter out the gravity waves but selection of an appropriate filter scale may be difficult.

Brooks (2003) developed an automated technique for retrieving estimates of the top and bottom of the local EZ at individual locations using a wavelet covariance transform, improving on the previous implementation, which estimated a single ML top (Davis et al. 2000), by using multiple wavelet dilations. This technique is less sensitive to mean vertical gradients in the background signal than gradient methods, which can be common under stable stratification where the inversion may not be well defined, and vertical gradients are common. Using multiple wavelet dilations it is possible to identify both upper and lower limits of the backscatter transition zone associated with the inversion, enabling more detailed information on the small-scale structure of the inversion and EZ.

It is clear from Figure 2.4.1, which shows a small part of a cross section of q, that area averaged estimates taken over a large domain cannot include information about the smaller scale processes which can contribute to entrainment. It is also obvious that area averaged estimates cannot include information about the variability of the EZ depth, which we will later see can tell us a lot about the dynamics of the EZ. This figure also gives a good example as to why the significant gradient method often gives such low estimate of EZ bottom; the central pocket of diluted ML air (yellow and green, at approximately 650m altitude and -500m in the horizontal), caused by entrainment, gives a large gradient in q and is identified as the EZ bottom, which is a false result.

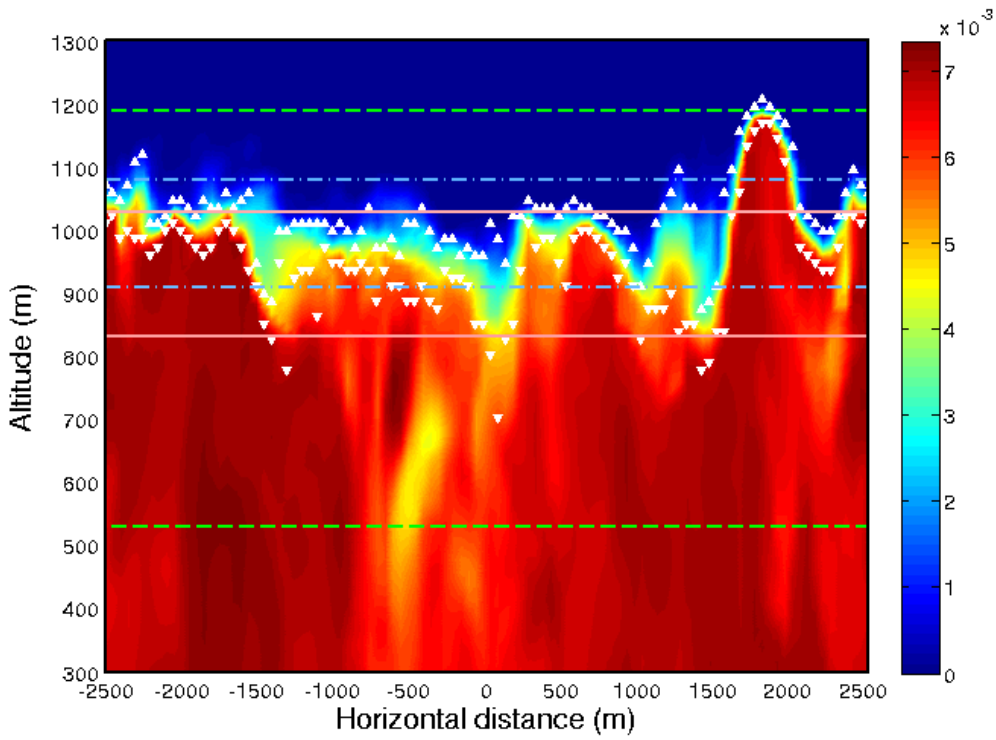

Figure 2.4.1. An example of a cross section of the water mixing ratio, q, with the estimation of the EZ depth by the different methods marked; 5-95% probability distribution (dash-dot blue), area of negative flux (solid red), significant gradient (dash green) and individual estimates of EZ top (white upward pointing arrows) and EZ bottom (white arrows pointing down) from wavelet analysis.

Other definitions which have also been used, include a measurement of the thickest continuous portion of a vertical column for which $7.5 \leq q \leq 8.5$ (gkg^{-1}), theses values represent the middle third of the jump between inversion and boundary layer values (Stevens et al. 2000). This definition will not be looked at any further in this study.

3. THE LARGE EDDY SIMULATION EXPERIMENTS

The Large Eddy Simulation (LES) was introduced in the 1970s by Deardorff (1974a, b). The LES code used here is the UK Meteorological Office's Large Eddy Model (LEM), version 2.3, which is a well established model that has been used to study entrainment in previous research (Lock and MacVean, 1999a, b). The vertical grid is stretchable allowing the area around the inversion to be studied at a high resolution and the outer region under a lower resolution to make the runs more time and cost efficient. Low resolution 2D simulations could be run first to locate the inversion and growth rate of the boundary layer so that the vertical grid for the 3D runs can be of maximum resolution around the inversion. However, for the runs used in this study, a high resolution grid, of approximately 12.5m in the vertical, was fixed around the area where the initial inversion was set, with the bottom of the high resolution grid situated 150m below the inversion and the top 600m above the height of the initial inversion to allow room for ML growth. A resolution of 25 m and approximately 115m in the vertical could be found below and above the inversion respectively. The horizontal resolution was fixed at 50m. The domain size was 4950×4950×3000m and the grid size was 100×100×100m. It is important that the domain size is large enough so that it does not limit the growth of the turbulent eddies. Figure 3.1. shows the initial set up of the model, which assumes that turbulence is strong enough within the mixed layer to maintain a constant potential temperature and water mixing ratio. At the inversion there is an increase in potential temperature, dependent on the run, which then increases at a constant lapse rate of 3K/km above the inversion. The temperature inversion is modelled as a finite depth and not a discontinuous jump as in some models. Simultaneously at the inversion the water mixing ratio decreases, from 10g/kg within the ML, to a constant value of zero above the inversion. For all runs except one, the ML height was set at an initial altitude of 650m and the initial inversion depth was 50m. Run 8i (see table 1 in appendixes) had this initial ML height reduced to 300m whilst retaining an initial inversion depth of 50m (see Appendix C).

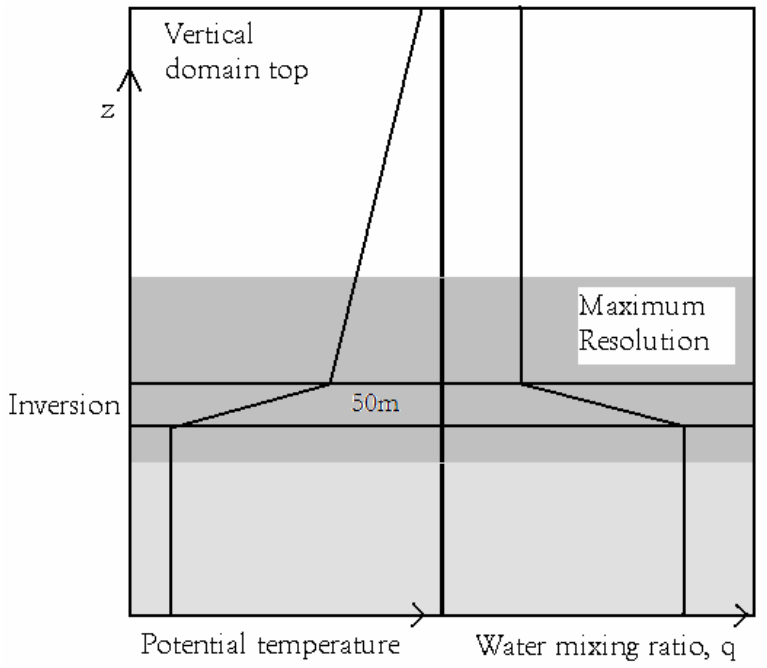

Figure 3.1. Initial set up of potential temperature, θ, and the water mixing ratio, q, profiles in the LEM. The area shaded dark grey represents the area of maximum resolution around the inversion.

In these experiments only the convective PBL is investigated, so turbulence is produced just by a surface heat flux with no wind shear present. It is also setup to simulate a cloud-free dry atmosphere, so the effects of moisture on the buoyancy of the air are not included, nor are the radiative effects of cloud top cooling.

Sensitivity tests have been carried out to determine the adequate resolution, at the inversion, needed to observe entrainment. In previous studies it has been found that the thickness of the inversion, the depth of the entraining eddies and the shape of vertical velocity spectra were determined mainly by the mesh spacing used (Stevens et al. 2000). These tests showed that increasing the horizontal resolution from 50 to 25 m would have little effect on the entrainment and decreasing the vertical resolution from 12.5 to 25 m around the inversion would affect entrainment, so this is avoided. However increasing the vertical resolution from 12.5 to 7 m may have improved results but due to time restraints the grid size of 50×50×12.5m was used throughout all runs. Appendix B gives the full results and analysis of these sensitivity tests.

A range of day-time conditions have been assured by having a variety of convective Richardson numbers (see section 4.1), by varying the inversion strengths and surface heat flux forcing. The initial inversion strength varied from a very weak inversion of a 1K jump

to a stronger inversion of a 10K jump. It is possible, in the atmosphere, for inversion strengths to reach upward of a 20K jump near coastal areas. The surface heat flux was varied from just $10W/m^2$ to $200W/m^2$, the surface heat flux is always positive representing convective conditions typical of the day-time when there is solar warming of the surface. Table 1 (see Appendix A) gives a summary of the runs used, including some key properties. The first two hours of data for each run have not been used, to allow time for the model to fully 'spin-up'.

In this study q is used as a passive tracer and assumed to be similar in behaviour to lidar backscatter from aerosols; this may not be totally accurate as some aerosols swell with water vapour making the change in concentration across the inversion more extreme, whereas q has been modelled as a conserved scalar quantity. It would, therefore, be beneficial to add into the model the effect of water on aerosols so modelled data can be compared to observed data from lidar backscatter of aerosols. However, more studies still need to be conducted on the aerosol composition of the atmosphere and entrainment zone, and how their chemical properties may be affected by the change in atmospheric properties within the EZ, such as moisture change. It may also be of interest to conduct a study into the affect of the wavelength used. In Faloona et al.'s (2005) study, observations of various 'conserved' scalars were used to investigate the entrainment process in the stratocumulus-topped boundary layer. They found the gas dimethyl sulphide (DMS) to be an 'almost ideal tracer of the marine boundary layer air because its only source is the ocean surface' so falls to near zero above the boundary layer, and it has a chemical lifetime 'comparable to the dilution timescale of the marine boundary layer due to entrainment' (Lenshow et al. 1999).

4. DESCRIPTION OF ENTRAINMENT EVENTS

4.1 Convective Richardson Number, Ri_*

To compare different PBL conditions, a Richardson number, is introduced. The Richardson number is a dimensionless number which can be used as a measure of dynamic stability to determine the existence of turbulence.

In this study the approach of Sullivan et al. (1998) is followed, in defining a convective Richardson number, Ri_*, which approaches the gradient Richardson number, Ri_g, as the limit of boundary layer thickness approaches zero. Ri_* contains factors similar to the bulk Richardson number, but where the velocities, temperatures, and depths are based on mixed-layer scaling parameters. In this study Ri_* is used instead of the bulk Richardson number as no wind shear is present. In previous work, the depth of the EZ and the entrainment rate have been found to relate to the convective Richardson number (Nelson et al., 1989) (see sections 5.1 and 5.3).

The following definition of Ri_* is used:

$$Ri_* = \frac{\Delta\theta}{\theta_*}, \qquad 4.1.i$$

where $\Delta\theta$ is the jump in potential temperature across the inversion which defines the inversion strength and θ_* is the mixed layer temperature scale,

$$\frac{\left(\overline{w'\theta'}\right)_s}{\left[\frac{gz_i}{\overline{\theta}}\left(\overline{w'\theta'}\right)_s\right]^{1/3}}. \qquad 4.1.ii$$

where g is gravity and $\overline{\theta}$ is the mean potential temperature within the PBL. It is therefore clear that increasing the surface buoyancy flux and decreasing the inversion strength will decrease the Richardson number and represent a BL which is becoming increasingly dynamically unstable and more turbulent.

If Ri_* is small, the interface is dynamically unstable and may become or remain turbulent, entrainment can occur without any influence from large eddies bellow. If Ri_* is large, there will be no entrainment unless the EZ is strongly influenced from below (Angevine, 2006). However, unlike the gradient Richardson number, a critical value is not well defined. Figure 4.1.1 shows the range of Richardson numbers used in this study; a large Ri_* is generally something larger than 40 and a small Ri_* is less than about 30.

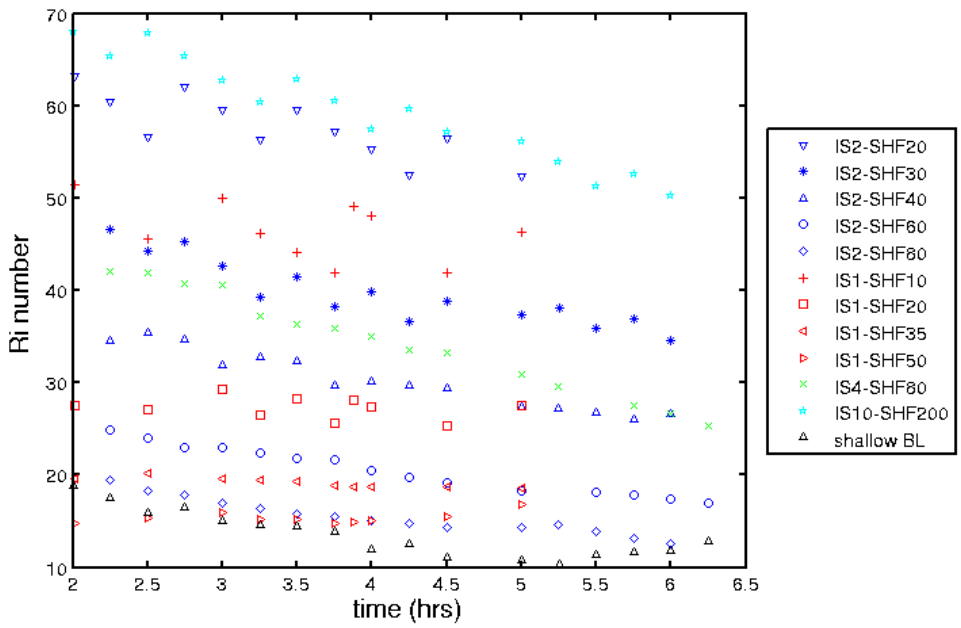

Figure 4.1.1.The Richardson number's evolution with time for different initial forcings from LEM model runs. IS# is the initial inversion strength of a jump of #K across the inversion and SHF# is a surface heat flux set to #W/m^{-2}. The run with the shallow boundary layer has an initial inversion strength of 2K and a surface heat flux of 40W/m^2, and the initial BL depth has been reduced from 650m to 300m (see table 1).

4.2 The current understanding of entrainment events

ML growth starts approximately half an hour after sunrise and reaches its maximum depth in the late afternoon (Stull, 1988) when the surface heat flux also reaches a maximum and thermals are at their most active. Buoyancy forces set up vigorous thermals resulting in non-local transport of heat and momentum; these dominate the convective PBL (Moeng and Sullivan, 1994). The temperature inversion, which occurs at the EZ, acts as a lid to the

rising thermals; restricting the domain of the turbulent structures and the growth of the ML. As the inversion strength is increased, less overshooting of thermals occurs and the entrainment rate decreases unless compensated for by a large surface heat force. Any entrainment that will occur in a BL which is strongly capped will be due to somewhat different mechanisms than entrainment at a weak inversion.

It has been concluded within a large amount of literature (Perera et al. 1994, Kit et al. 1997) that entrainment mechanisms are dependent on a measure of the local Richardson number $Ri_l = N_i^2 L_H^2 / u_H^2$, where Ni is the buoyancy frequency of the inversion, and L_H and u_H^2 are the integral length scales and variance of the turbulence in the absence of the density interface. Sullivan et al. (1998) studied entrainment and the structure of the inversion layer of a clear convectively driven PBL over a range of convective Richardson numbers, similar in magnitude to these presented here, using a LES model. It was found that for low Richardson numbers, thermal plumes led to a folding of the interface, causing entrainment. As the Richardson number increases and the stability of the PBL also increases, there is a shift towards entrainment caused by strong horizontal and downward motion near the plumes edge, which pull pockets of warm air down into the PBL which are then entrained by turbulence within the PBL. The reason for this change was that at a weak inversion, as a thermal plume rises the temperature contours are lifted and compressed at the head of the plume. This leads to an increase in the stratification which eventually stops the plume rising any further and the plume is deflected sideways and then downwards resulting in entrainment, as the free tropopause air is engulfed by the folding interface. Conversely if the inversion layer is stronger, large-scale folding is prevented and the interaction between the turbulent thermals and the overlying inversion leads only to local distortions of the inversion layer and local pockets of warm air are stretched out and eventually entrained by turbulence within the PBL.

Similarly, Stull (1988) grouped entrainment into two different scales; that of lateral entrainment by small eddies into the side of thermals and vertical entrainment, which occurs on the thermal scale into the whole of the ML. These relate to Sullivan et al. (1998)'s description of entrainment at a low Richardson number and a high Richardson number respectively. In Section 5.2 a study of the variability of the EZ top and bottom will be conducted to see if this can be used to directly infer a measure of the Richardson number from BL measurements, and from Sullivan et al. (1998) tell us something about the entrainment process.

4.3 Statistics of 'upwellings' at the ML top, z_i.

From the previous section it is clear that 'upwellings' are associated with the top of a rising thermal and have the effect of locally increasing the thermal stratification at the inversion until they can rise no more. Figure 4.3.1. shows a time profile of the percentage of 'upwellings', across the horizontal domain, for a variety of Ri_*, achieved by increasing the surface heat flux (SHF) and keeping a constant inversion strength (IS). For the run IS2-SHF20, Ri_* is very high, representing a very stable PBL. For this initial setup there is a distinctive 'saw-tooth' pattern, this smoothes out as the surface heat flux is increased and the PBL becomes more and more unstable. This suggests that for an 'upwelling' to occur in a very stable PBL, which may lead to entrainment, there needs to be a large build up of energy first, and then, when entrainment occurs, there is a sudden expenditure of energy. This is verified by Figure 4.3.2. which compares the change in the percentage of 'upwellings' with time, with the change in the maximum vertical wind flux, $\overline{(w'w')}_{\max}$. $\overline{(w'w')}_{\max}$ can be used as an estimate of the turbulent kinetic energy (TKE= $\frac{1}{2}\rho U^2$, where $U^2=(u')^2+(v')^2+(w')^2$) as density is assumed constant and turbulence is mostly isotropic, so there is no need to include horizontal wind fluxes. There is a similar 'saw-tooth' pattern in the maximum vertical wind variance, indicating the hypothesised store of energy and then a sudden expenditure of energy in the form of entrainment may be valid. As the BL becomes more unstable there is a much smoother and faster growth in the energy available in the BL. There is also slight evidence of a 'saw-tooth' pattern of Ri_* with time which smoothes out as Ri_* decreases, see Figure 4.1.1. The value of Ri_* where there is a transition between the 'saw-tooth' and smooth evolution with time appears to decrease as the inversion strength decreases; which implies that this build up of energy that is needed to drive the entrainment has a direct link with the strength of the inversion. However, as seen in Figure 4.3.1. the peaks do not occur at the same point in time, suggesting hystereris.

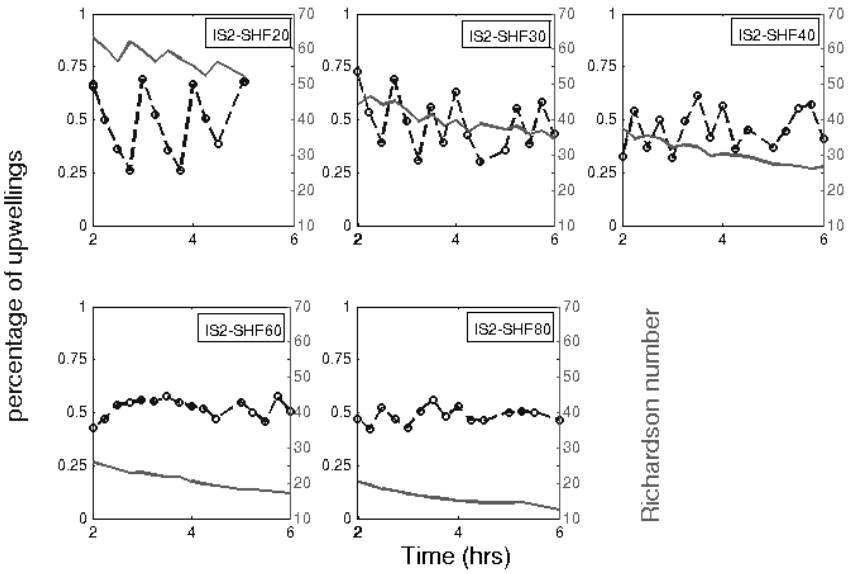

Figure 4.3.1. A comparison of how the percentage of higher than average ML tops (**- -o**), or 'upwellings', changes with time compared to the convective Richardson number (solid line), for different initial surface heat fluxes.

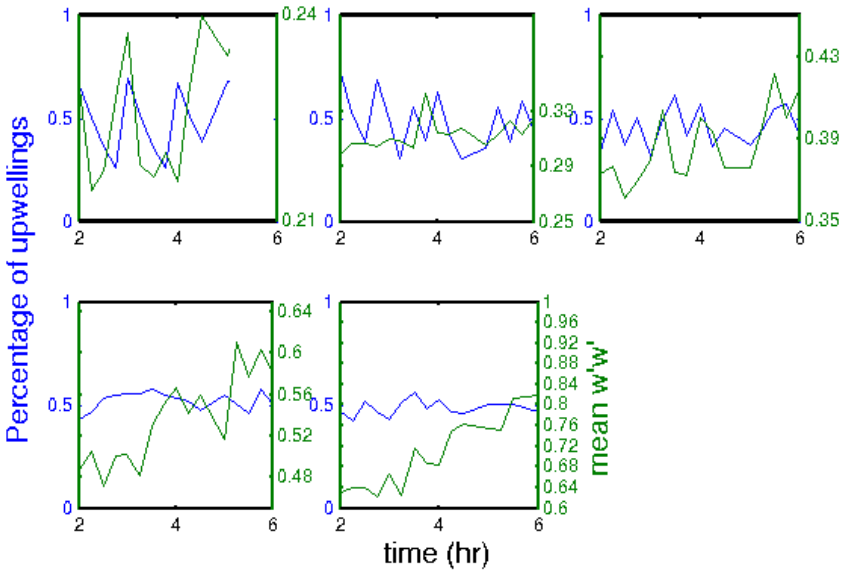

Figure 4.3.2. Comparison of time profiles for the percentage of upwellings (blue solid line) and the maximum vertical wind flux, $\left(\overline{w'w'}\right)_{\max}$ (green solid line), used as an estimate to the turbulent kinetic energy. Note that each plot of the maximum in vertical wind flux does not use the same scale.

In the stable PBL, the 'saw-tooth' pattern in percentage of upwellings with time (Figure 4.3.2) indicates a ML top that is alternating between a large percentage of lower than

average tops which must then be balanced out by a few extremely high tops and then the opposite, implying that entrainment is only occurring in a very localised area. The smoother results seen as the surface forcing becomes stronger, suggest that entrainment is perhaps occurring on a larger spatial scale or it is happening on a smaller time scale, as enough energy for entrainment does not take so long to build up, and the sampling of times used (maximum 15min) may not be small enough to capture individual entrainment events.

Speculation that the variability of the percentage of 'upwellings' may be time dependent is tested in Figure 4.3.3. A PBL with a low Ri_* has been simulated twice using the same initial setup (IS2-SHF60), once with the original low time output of a maximum of 15 minutes, and the second with a high time output of every 2 minutes at its peak. For time efficiency the second has only modelled 2D slices of the original. In Figure 4.3.3 the original (**solid line)** is compared with 2 different vertical slices (**dash-dot line** and **dash line**). It is clear that the smoothness in the time profile of the percentage of 'upwellings' at a low Ri_* was caused by the time step being too large and averaging out a high frequency 'saw-tooth' pattern, which does suggest that the entrainment at a low Ri_* is happening on a much smaller time-scale. This is as expected in a very turbulent atmosphere where entrainment can occur spontaneously. However, the standard deviation has not changed significantly so does not have a large effect on the future results (Figure 4.3.7.).

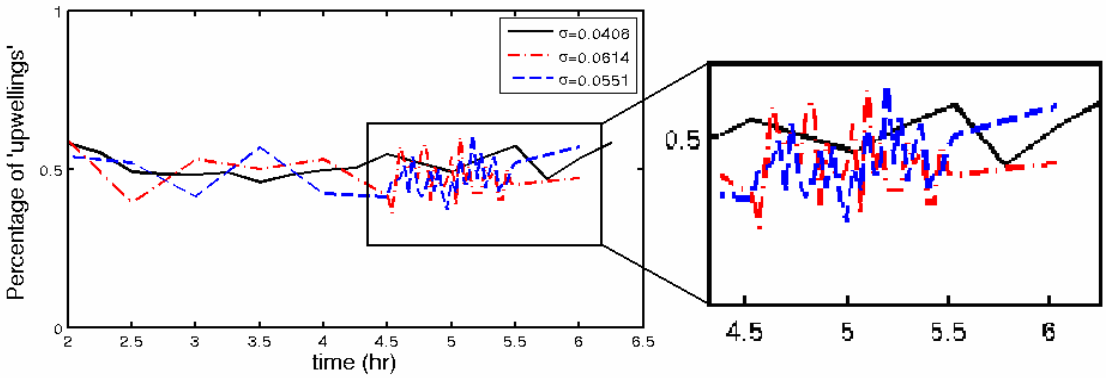

Figure 4.3.3. Sensitivity test of the percentage of 'upwellings' for an increase in the time resolution. Original IS2-SHF60 run (**solid line**), with maximum output of 15 minutes, compared with estimates of the percentage of 'upwellings' from 2D sections of the same run with maximum output of 2 minutes between 4.5 and 5.5 hours (**dash-dot line** and **dash line**).

For a PBL with a high Ri_* there will be large areas of higher (or lower) than average ML tops which are balanced out by only small isolated areas of extreme low (or high) ML tops there will however also be much less variability in the actual heights of the ML top. Figure 4.3.4 shows that the ratio of upwellings to downwellings moves away from 0.5 as Ri_* is increased and the PBL becomes more stable. Figure 4.3.5 shows that although the distribution of upwelling and downwelling is more even for a low Ri_*, the variability of the ML top is much greater due to an increasingly weaker inversion which is much easier to distort by the rising thermals.

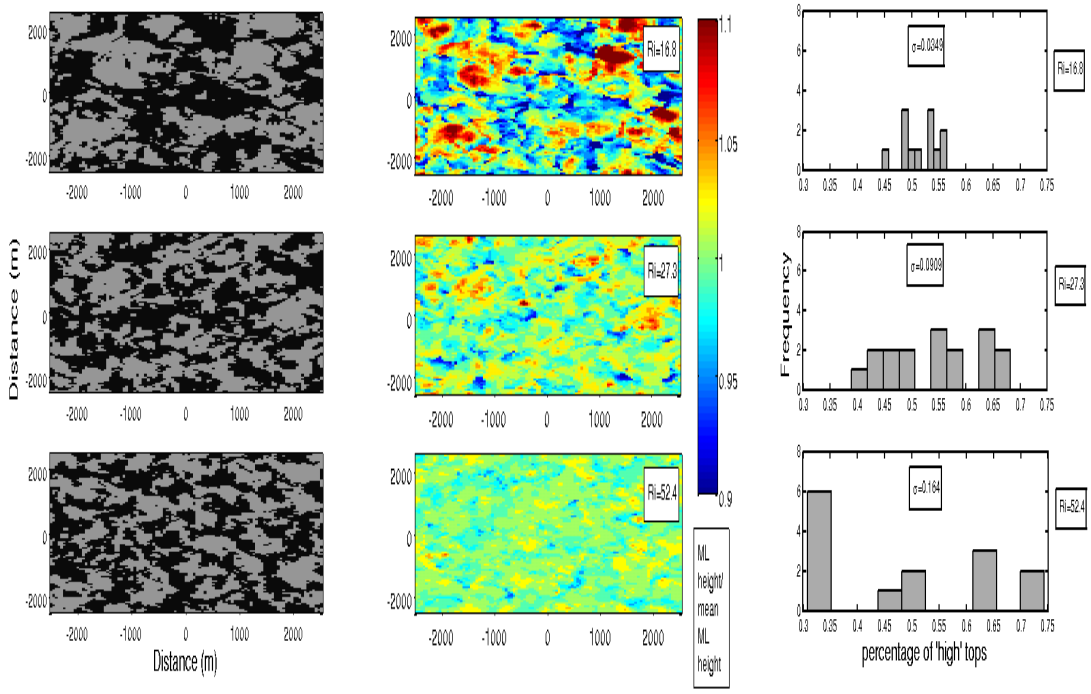

Figure 4.3.4. (left) Distribution of 'upwellings' (dark) and 'downwellings' (light), for a range of Ri_*. **Figure 4.3.5**. (middle) Magnitude of upwellings and downwellings, for a range of Ri_* (>1 is a downwelling (reds), <1 upwelling (blues)). **Figure 4.3.6.** (right) A histogram of the percentage of 'upwellings' for a low (top), medium (middle) and high (bottom) Ri_*.

Figure 4.3.6, shows that for a low Ri_* there is little spread in the percentage of upwellings as there are nearly always 50% upwellings and 50% downwellings. As Ri_* increases so does the spread in values of the percentage of upwellings.

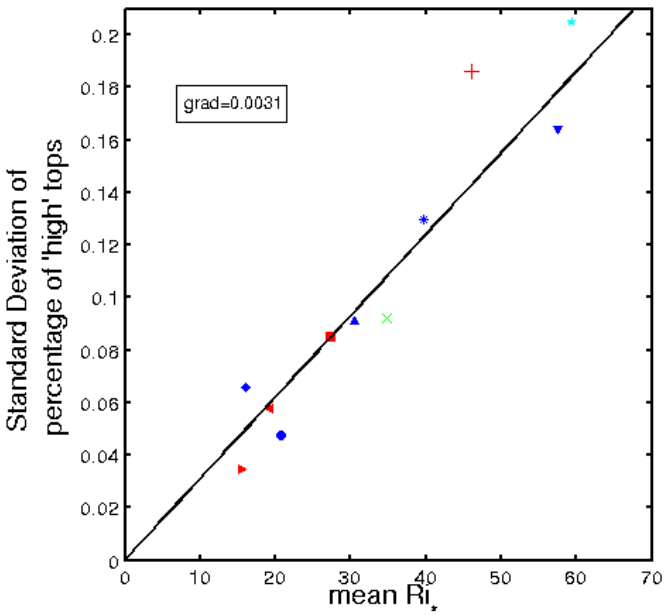

Figure 4.3.7. Standard deviation of high tops (explained in Figure 4.3.1.) as a function of convective Richardson number. Symbols are defined in the same way as on Figure 4.1.1.

In Figure 4.3.7. the standard deviation of the percentage of high tops is plotted as a function of Ri_*. It is important to note, however, that this is not a measure of the variability in the ML height, but a measure of the variability of percentage of upwellings. It is clear that the relationship seen in Figure 4.3.6, is strongly linear, so the variability of the percentage of 'upwellings' occurring across the horizontal domain is directly linked to the turbulent structure of the PBL.

5. PARAMETERIZATIONS

Parameterization of the EZ is very important, as the entrainment velocity is a 1st order term in the budgets of heat, moisture, momentum and pollutants. Forecast models are too low in resolution to directly include the small-scale processes which can lead to entrainment.

5.1 Entrainment Zone depth

Comparison of definitions

Comparisons of the definitions of the EZ depths discussed in Section 2 will now be conducted. To make comparisons between the EZ depths under different initial conditions, the EZ depth has been normalised by the mean ML depth, z_i, determined by the maximum in the gradient of q. It is found for all definitions that the normalised EZ depth, Δh, is inversely proportional to the convective Richardson number, Ri_*, (see Figures 5.1.1 and 5.1.2)

$$\frac{\Delta h}{z_i} \propto Ri_*^{-1} \qquad 5.1.i$$

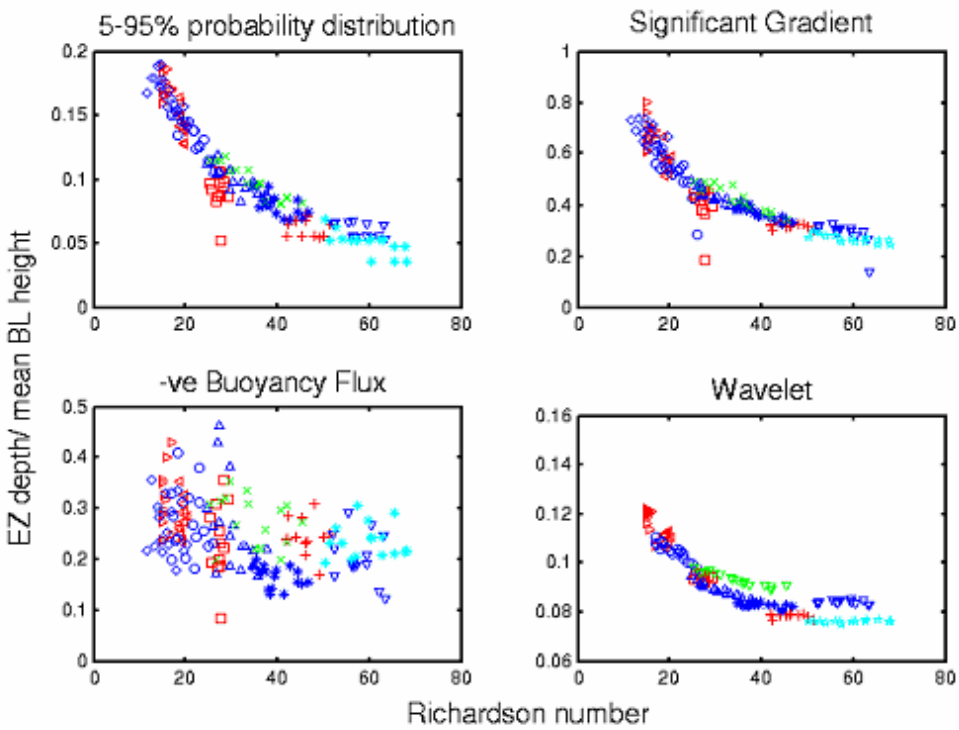

Figure 5.1.1. The four different definitions of EZ depth plotted as a function of Ri_*. Symbols are defined in the same way as on Figure 4.1.1.

This is in good agreement with past literature, Stull (1973), Zeman and Tennekes (1977). In these studies equation 5.1.i came about from the use of the momentum balance equation to calculate the thermal overshoot distance, *d*, as a function of its initial upward velocity (assumed proportional to the convective velocity scale, w_*) and the strength of the capping inversion. Then, assuming the EZ depth is proportional to *d* gives the relationship we have observed (5.1.i). This relation predicts that the EZ depth will never be zero and that as $Ri_* \rightarrow 0$, EZ depth $\rightarrow \infty$, which is not physically meaningful. So 5.1.i can only be valid in this range of convective Richardson numbers.

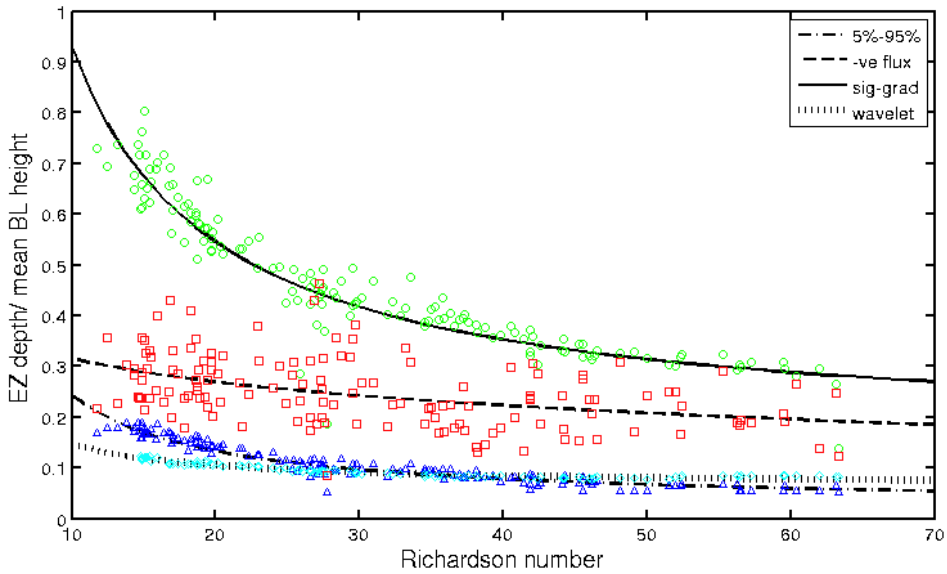

Figure 5.1.2. The four defined EZ depths, normalised by the mean ML depth, plotted as a smoothed inversely linear function of Ri_*. (5-95%: blue triangles, -ve flux: red squares, sig-grad: green diamonds, wavelet: cyan circles)

The smoothed functions plotted in Figure 5.1.2 can be described as:

$$\frac{\Delta h_{5-95}}{z_i} = \frac{2.2}{Ri_*} + 0.023$$
$$\frac{\Delta h_{flux}}{z_i} = \frac{1.7}{Ri_*} + 0.18$$
$$\frac{\Delta h_{sig_grad}}{z_i} = \frac{7.7}{Ri_*} + 0.16 \qquad \text{5.1.ii (a-d)}$$
$$\frac{\Delta h_{wavelet}}{z_i} = \frac{0.82}{Ri_*} + 0.064$$

Where $\Delta h_{5\text{-}95}$ is the EZ depth estimated by the 5-95% limits of the probability distribution of the maximum gradient seen in a conserved scalar quantity, Δh_{flux} is the EZ depth estimated by the horizontally averaged area of negative buoyancy flux, Δh_{sig_grad} is the EZ depth estimated by the area of significant gradient of a horizontally area-averaged conserved scalar quantity and $\Delta h_{wavelet}$ is the EZ depth estimated by the wavelet analysis of a conserved scalar quantity.

The relations, 5.1.ii (a-d), can be compared to Gryning and Batchvarova (1994) who found, $\frac{\Delta h}{z_i} = \frac{1.13}{Ri_*} + 0.2$ using data from laboratory experiments (Deardorff et al, 1980) and observational data (Boers and Eloranta, 1986), where Δh is now the EZ depth defined by the horizontally averaged area occupied by 10-90% clean air from the FA. This predicts a deeper EZ than predicted by our model for Δh_{sig_grad} which uses a similar definition of the EZ but has a much shallower gradient; this highlights the importance of choice of significant gradient in q.

It is clear from Figures 5.1.1 and 5.1.2, that the wavelet defined EZ depth has the most robust relationship with Ri_* and the area of negative buoyancy flux defined EZ depth has the least. The 5-95% and significant gradient definitions both have a good relationship with Ri_* but the significant gradient method produces more outliers which are clearly false results created by large background gradients at altitudes lower than the true EZ height. These could be removed but this is time consuming and would decrease the amount of data available. The large variability of the EZ depth defined as the area of negative buoyancy flux and its lack of dependence upon Ri_*, compared to the other definitions, is due to this EZ depth estimate being a measure of instantaneous entrainment events, whilst the others are measuring the cumulative effect, on the concentration of q, of previous entrainment events.

The increase in magnitude of the gradient between the wavelet estimate, probability distribution estimate and significant gradient estimate is evidence of the very different properties being measured. The wavelet method takes individual estimates of the EZ top and bottom and then average across the whole domain, similarly the 5-95% method takes individual estimates of the ML top and then looks at the probability distribution limits; whilst the flux and significant gradient methods make estimates of the EZ top and bottom from horizontally area averaged properties. The large spread in values of the EZ depth estimated from the flux and significant gradient methods would make it impossible to estimate Ri_* from these estimates of the EZ depth, emphasising the problem with using area averaged values to make measurements on the EZ. From now on we will only be using EZ top and bottom values estimated by the wavelet analysis method.

5.2 Wavelet statistics of the entrainment zone

Some studies have been conducted in to the statistics of the ML top, z_i, namely Sullivan et al. (1998), which found the standard deviation of z_i to be inversely proportional to Ri_*. It was also found that the relationship between the skewness of zi and Ri_* was dependent upon the strength of the inversion. However, until now the statistics of individual estimates of the EZ top and bottom have not been studied which is now possible using Brooks (2003) wavelet technique. The distribution of individual estimates of the top and bottom of the EZ may be related to Ri_*, creating a new way to parameterize the EZ. In a rapidly entraining PBL, entrainment is caused by strong overshooting thermals from the ground, making the inversion get weaker and weaker allowing more and more entrainment. Entrainment in these turbulent PBLs is less uniformly distributed and can occur sporadically and instantaneously. Where as in a more stable PBL there is less energy to drive thermals and a strong capping inversion impairs the thermals ability to overshoot meaning entrainment that does occur happens over a larger time scale, as seen in section 4.3, and will not distort the ML top as severely, see Figure 4.3.5. Figure 5.2.1 illustrates the increasing spatial variability in the EZ top and bottom as Ri_* decreases. It can also be seen that the EZ bottom generally varies more than the EZ top, as the rising thermals which are causing the entrainment will have the most energy at the EZ bottom before they begin to become impaired by the temperature inversion.

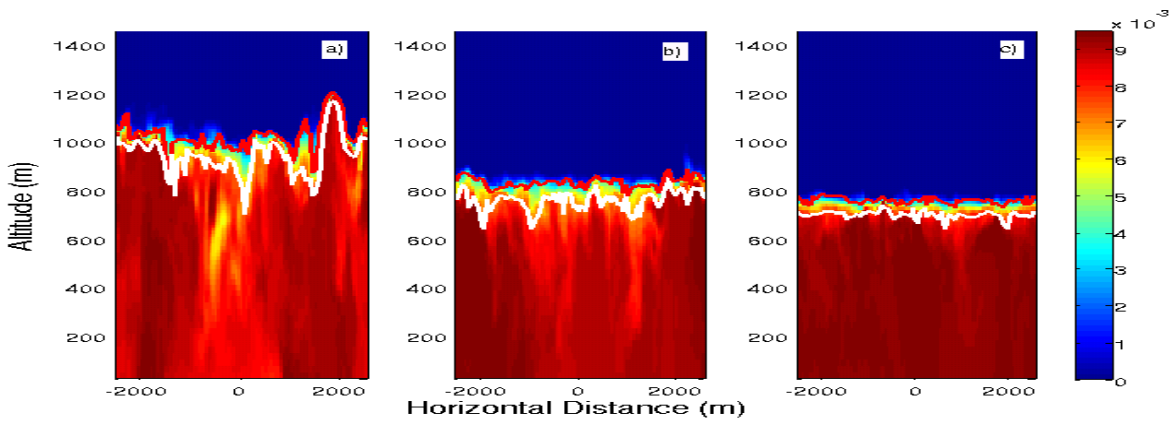

Figure 5.2.1. Cross sections of water vapour mixing ratio, q. The thick white line shows the variability of EZ bottom and the thick red line shows variability of EZ top, both estimated by the wavelet technique. These are compared across a range of Ri_*; a) low Richardson number b) medium Richardson number c) high Richardson number.

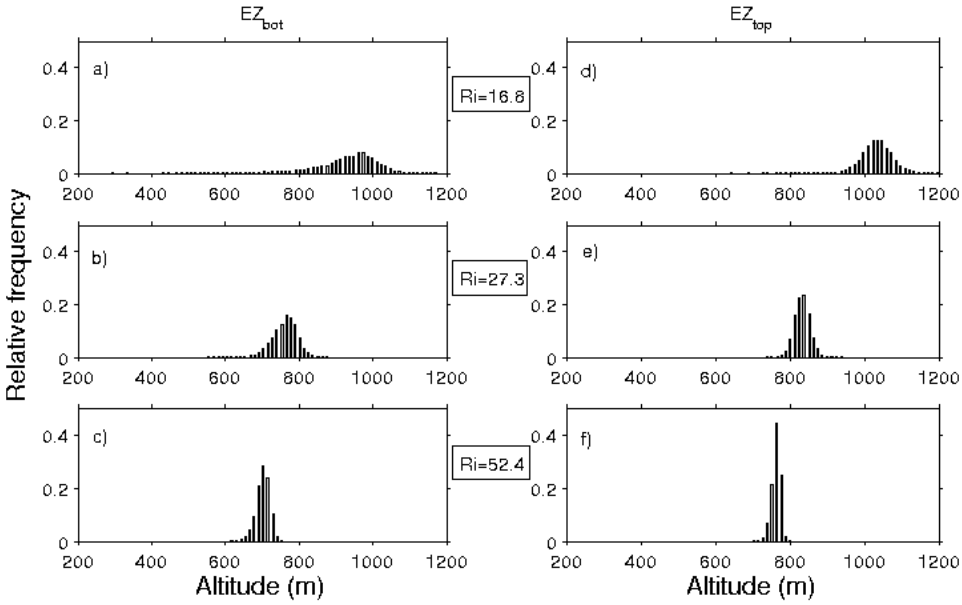

Figure 5.2.2. Probability distribution of EZ top (right) and EZ bottom (left) for a range of Richardson numbers.

Examples of the probability distribution of the EZ top and bottom are shown in Figure 5.2.2. As well as the increasing variability of the individual EZ top and bottom estimates, Figure 5.2.2 shows that the shape of the distribution, or skewness (deviation from a normal distribution), also changes as Ri_* decreases. As Ri_* becomes smaller the distribution gets increasingly negatively skewed as long tails of very low estimates of EZ bottom occur.

In Figure 5.2.3 the skewness of the EZ top (black symbols) and bottom (blue symbols) are plotted as a function of Ri_*. It is clear to see that for Ri_* greater than 20, for both EZ top and bottom there is an approximately linear relationship with Ri_*. However, the two are visibly different; the gradient for EZ bottom is distinctly positive whilst the gradient for EZ top is equally distinctive as negative and also slightly larger in magnitude than that of the EZ bottom. These two lines cross when Ri_* is approximately 60, indicating a change to a slightly more skewed EZ top than bottom for a very stable BL, however both are negative. For Ri_* less than 20, this pattern is no longer followed and the values of skewness spread out, for the EZ bottom the skewness becomes very negative, and for the EZ top the skewness values spread out in both negative and positive directions. So, for a very turbulent BL, the EZ bottom has a large spread of lower values than the bulk and the EZ top may equally be positively or negatively skewed, or show no skewness at all. For PBLs where Ri_* is less than 60 the consistently higher values of skewness for EZ top compared to the EZ bottom implies that distribution of values of the EZ bottom are less

centred on the mean height. This implies that deep entraining downdrafts are having a greater affect on the EZ bottom and this is becoming greater as the BL becomes increasingly unstable.

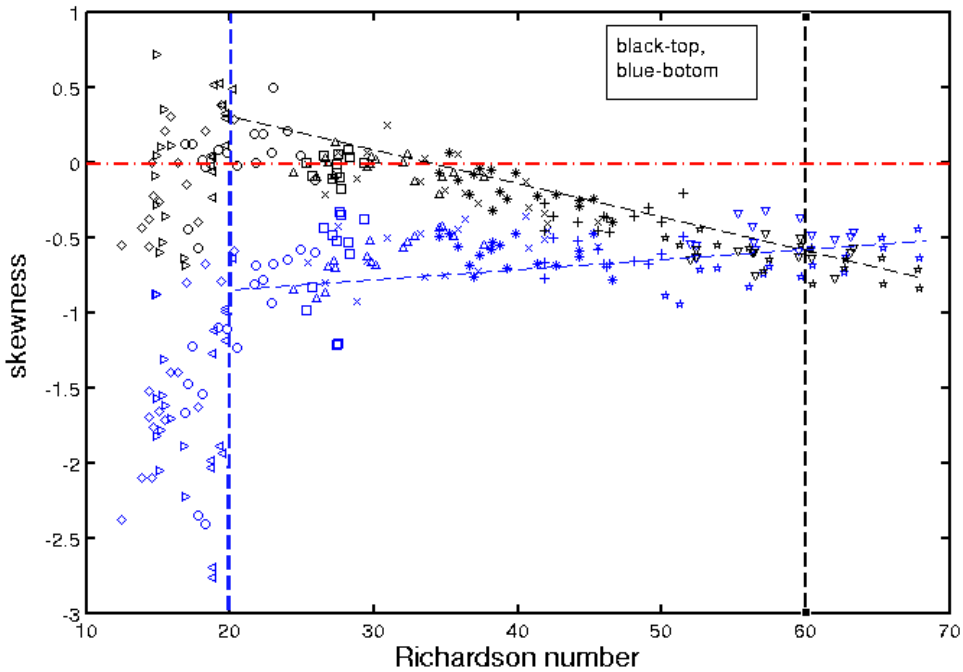

Figure 5.2.3. The skewness, S, of the distribution of EZ top (black) and bottom (blue) plotted as a function of Ri_*. The red dash-dot line at S=0 represents a normal distribution, centred on the mean.

The standard deviation, σ, of EZ top and bottom have similarly been plotted against Ri_* in Figure 5.2.4. This appears to be a smoother and stronger relationship than skewness as a function of Ri_*, and the variability of EZ bottom is consistently higher than the variability of the EZ top. However, the values of standard deviation for the EZ top and bottom become increasingly close as Ri_* increases and the inversion becomes stronger and less deep. The standard deviation of EZ top and bottom may be a very significant parameter, as if the standard deviation is zero, there is no variation in the estimates of EZ top and bottom and this could be used as a measure of whether entrainment is occurring or not.

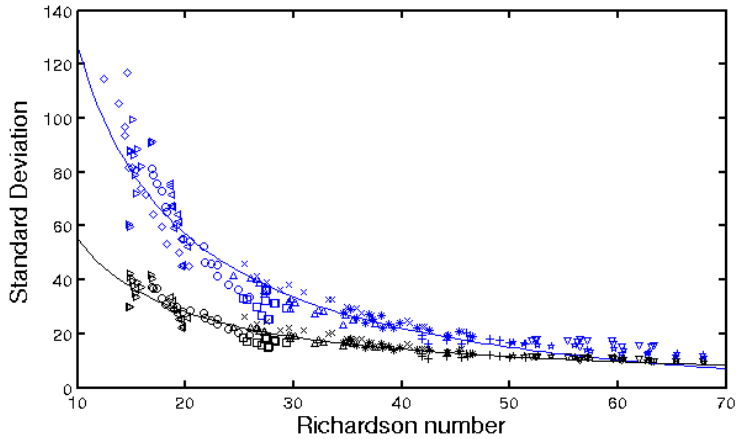

Figure 5.2.4. The standard deviation of the EZ top (black) and bottom (blue) plotted as function of Ri_*.

The difference between the statistics for EZ top and bottom are shown in Figures 5.2.5 (skewness) and 5.2.6 (standard deviation). These, again, both have a strong relationship with Ri_* and show that the relationship between the statistics of the EZ top and bottom are a consistent function of the stability of the PBL.

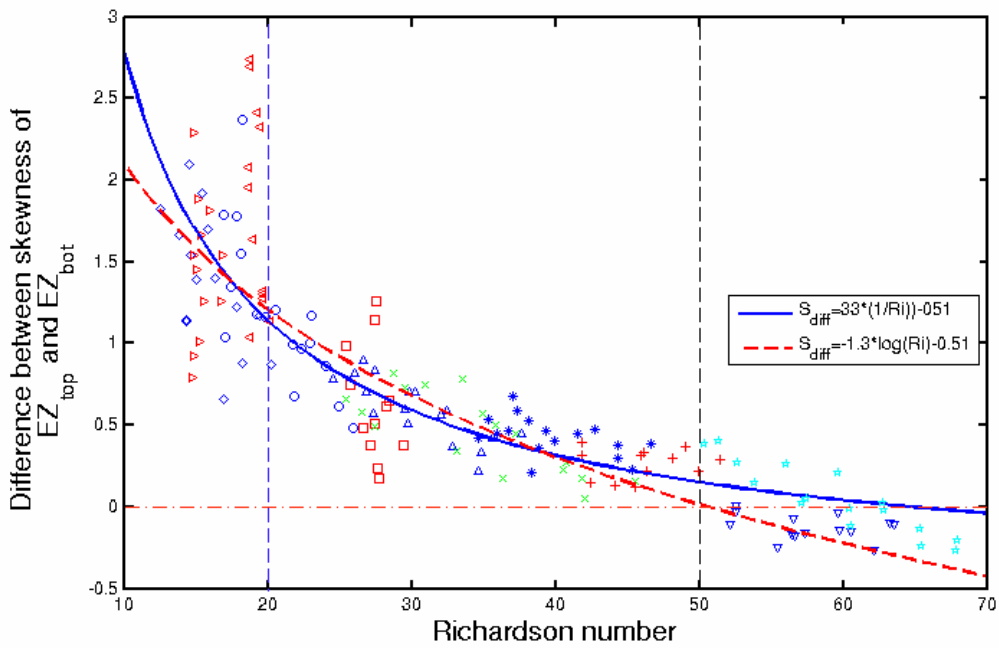

Figure 5.2.5. The difference between the skewness of the EZ top and EZ bottom plotted as a function of Ri*. An inverse linear (---) or logarithmic (- - -) relationship is suggested.

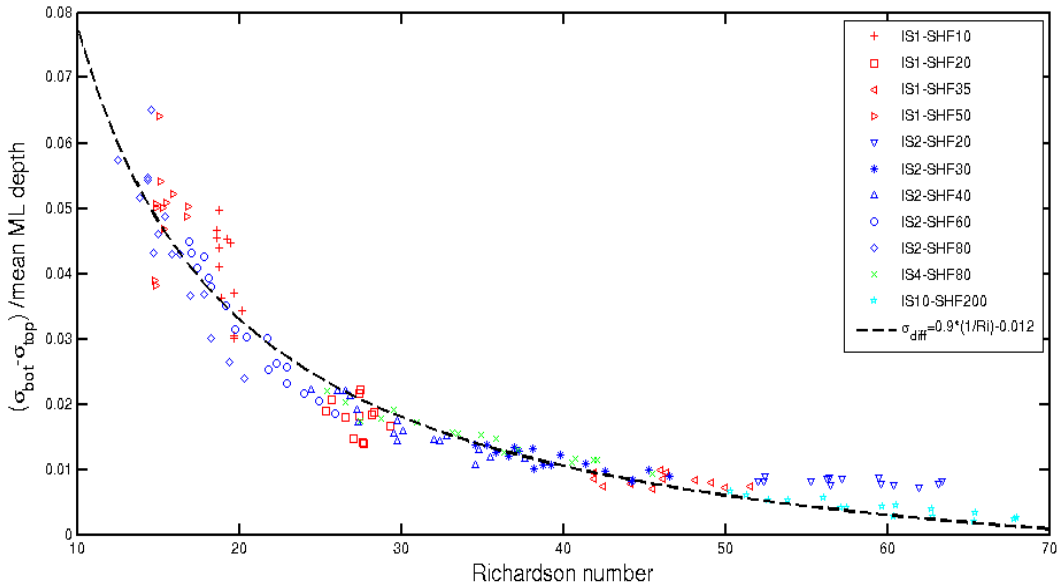

Figure 5.2.6. The difference between the standard deviation of the EZ top and bottom, normalised by the mean ML depth, plotted as a function of Ri_*. The line of best fit (- - -) suggesting an inversely linear relationship, has also been marked.

The robustness of the relationship shown in Figure 5.2.6 is convincing enough to suggest that it is possible to deduce an estimate of Ri_* from simply knowing the difference between the standard deviations of the EZ top and bottom, using the wavelet algorithm. These values have now been normalised by the mean ML depth, assumed to be the altitude of the maximum gradient in q, to subtract any influence a varying ML height may have. From this observation the following relationship may be hypothesised:

$$\frac{\sigma_{bot} - \sigma_{top}}{z_i} \propto Ri_*^{-1} \qquad 5.2.i$$

This relationship appears to hold for all inversion strengths, and over our full range of Ri_*.

This result is significant for the analysis of lidar data obtained from ground, aircraft and newly available satellite based profilers; such as CALIPSO (Cloud Aerosol Lidar and Infrared Pathfinder Satellite Observations) which will fly in tandem with the CLOUDSAT radar satellite as part of the A-train; both will be dedicated to the observation of clouds, aerosols and the water cycle. From the lidar backscatter profiles produced, wavelet analysis can be applied routinely, processing the large amounts of data available, to give estimates of the EZ top and bottom and in turn, via the relation 5.2.i, a good prediction of the Ri_*

and the stability of the PBL. This could then be used to describe the mechanisms responsible for entrainment and the time and spatial scales on which it is happening. Furthermore, the convective Richardson number has been used as a major factor in many parameterizations of the PBL, so this direct relationship with an easily measurable parameter may make it now possible to deduce such important factors as the entrainment velocity, w_e, from easily obtained measurements.

5.3 Entrainment velocity, w_e.

As seen in the previous sections the entrainment velocity is an important parameter in forecasting the distribution of clouds, the dilution and transportation of pollution from a ground source and the potential temperature of the PBL, to name but a few. However, the entrainment rate cannot be measured directly so must be parameterized in terms of other measurements.

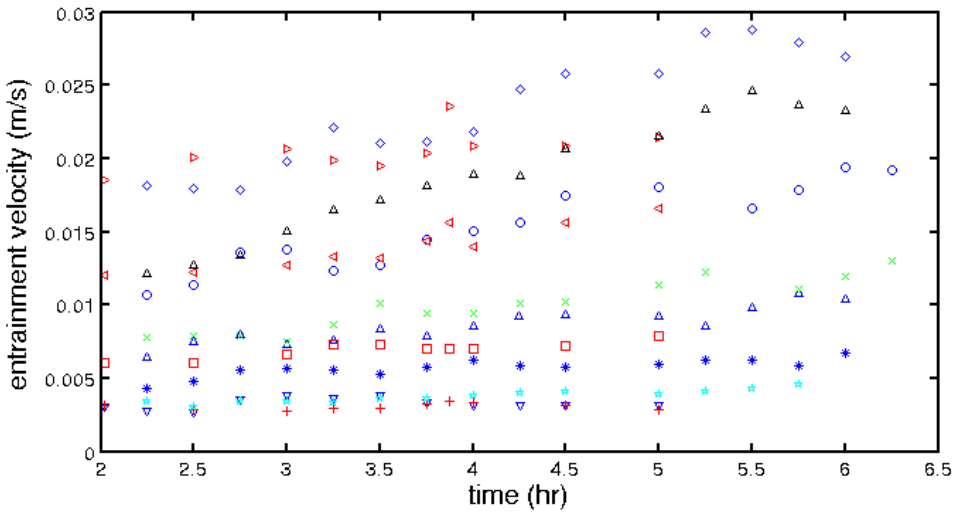

Figure 5.3.1. Evolution of entrainment velocity with time, for LEM runs with different initial forcings, see previous figure for symbol meanings

Entrainment velocity, w_e, is governed by the turbulent intensity and the strength of the capping inversion. In Figure 5.3.1 this is illustrated. It is also noticeable that for the runs with a lower Richardson numbers the entrainment velocity increases at a faster rate, as the inversion strength becomes weaker, and this increase with time becomes less smooth. Deardorff et al. (1980) found, for Richardson numbers typical for the atmosphere, the relationship between the entrainment rate and Richardson number to be:

$$\frac{w_e}{w_*} = \frac{A}{Ri}, \qquad 5.3.i$$

where w_e is the entrainment velocity and A is a parameter in the range $0.1<A<0.2$ which varies with shear (Moeng and Sullivan 1994). However, Figure 5.3.2 shows that for these simulations the relationship between entrainment rate and Ri_*^{-1} is linear, but the gradient, A, may be some function of the inversion strength, $A_{\Delta\theta}$, with $A_{\Delta\theta}$ ranging from 0.14 to 0.27.

$$\frac{w_e}{w_*} = A_{\Delta\theta} Ri_* \qquad 5.3.ii$$

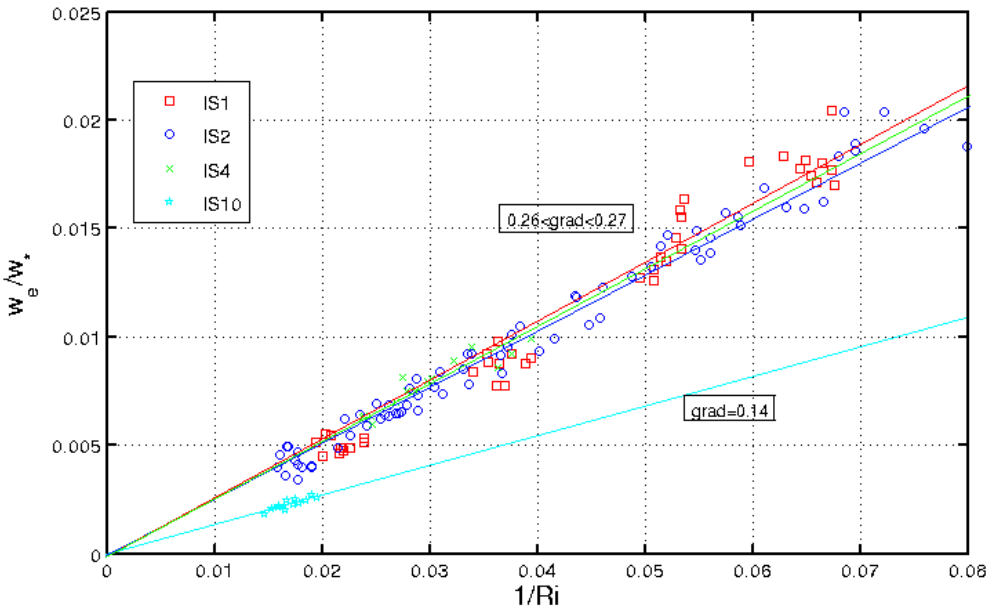

Figure 5.3.2. Comparison of normalised entrainment rate, grouped by strength of the inversion layer, vs. Ri_*^{-1}.

An entrainment rate parameterization developed from the layer-averaged conservation equation for potential temperature, assumes that the potential temperature and the buoyancy flux undergo a jump at the inversion layer, giving:

$$w_e \Delta\theta = -\overline{w\theta}_{\min} + \Delta h \frac{\partial \hat{\theta}}{\partial t}. \text{ (Betts, 1976)} \qquad 5.3.iii$$

where $\hat{\theta}$ is the average potential temperature within the inversion zone. Using our defined Ri_* this can be rewritten as:

$$\frac{w_e}{w_*} = \frac{1}{Ri*}(A_{w\theta} + A_{\Delta h}), \qquad 5.3.\text{iv}$$

Where the buoyancy flux parameter $A_{w\theta} = -\overline{w'\theta'}_{\min} / \overline{w'\theta'}_s$ and the inversion-layer thickness parameter $A_{\Delta h} = (\Delta h / \overline{w'\theta'}_s)\partial\hat{\theta}/\partial t.$ As can be seen in Figure 5.3.1, a strong capping inversion reduces entrainment and a strong surface buoyancy flux increases entrainment. Sullivan et al. (1998) found this to be a good fit to their data as, for clear convective PBLs, entrainment rate parameterizations derived from a jump model should account for the finite thickness of the inversion layer, Δh, and models which predict A to be a constant do not allow for this. $A_{w\theta}$ is often taken to be 0.2, but can range from 0.1 to 0.5. This ratio is assumed to be equal to the ratio of inversion depth to ML height. As the ML grows so does the EZ depth, and it is assumed that the ratio of these two depths remain constant.

Equations 5.2.i and 5.3.i give:

$$\frac{w_e}{w_*} = A_\sigma \frac{\sigma_{bot} - \sigma_{top}}{z_i} \qquad 5.3.\text{v}$$

where A_σ is a positive parameter and possibly a function of the inversion structure. Further studies need to be conducted into the exact nature of A_σ..

6. CONCLUSIONS

As many studies have already found, the mechanisms responsible for entrainment are dependent upon the turbulent nature of the PBL which can be represented by a measure of the convective Richardson number. Here, studying the distribution and ratio of upwellings gave an insight into the time and spatial scales responsible for entrainment. It is clear that when the PBL is capped by a strong inversion a large amount of energy must be available for a thermal plume to penetrate the inversion layer. This causes a build up of energy in the ML before entrainment can occur which then brings about a large expenditure of energy so energy must then build up again before another episode of entrainment can happen. The time-scale of this process was seen to decrease as the Richardson number decreased. It was also found that as the Richardson number decreased the area of the upwellings increased which explained the change in the distribution of the percentage of upwellings. Assuming that the percentage of upwellings is directly proportional to the area of the upwellings then it can be concluded that the area of the upwelling has a linear relationship with the convective Richardson number, see Figure 4.3.7.

A large part of the motivation for this study has come from the need to find a robust and meaningful definition of the EZ. This study has enabled the conclusion that the EZ depth cannot be estimated using area average values as the entrainment which is responsible for the finite depth occurs on a very localised scale. Defining the EZ using area averaged estimates proved to be inconsistent with the convective Richardson number, which has been used as a measure of the turbulent structure of the PBL. The two definitions based on local measurements proved to have strong correlations with the inverse of the convective Richardson number. However, the wavelet based method showed to be the most practical in the study of the EZ. This was mainly due to the wavelet methods unique ability to produce individual estimates of the EZ top and bottom allowing a more in depth study of the EZ structure to be carried out. This definition was also the least ambiguous; the flux method was seen to have difficulties in defining the EZ top, the significant gradient method used an arbitrary choice of what was deemed 'significant' and often predicted too high an EZ depth based on background gradients in the profile, and the probability distribution had problems when choosing the percentile limits. Unfortunately the area of negative flux is thought to be the most meaningful estimation of the EZ depth,

and part of the drive of this study was to find a link between the area of negative flux and a more easily measured estimate of the EZ depth. However, the lack of dependence of the area of the negative flux with the convective Richardson number makes it currently impossible to relate the wavelet defined EZ depth back to this more physically meaningful definition. As seen in Figure 6.1 there is a very poor correlation between these two estimates. More studies into the EZ depths are hence still necessary, to remove the current ambiguity in entrainment studies.

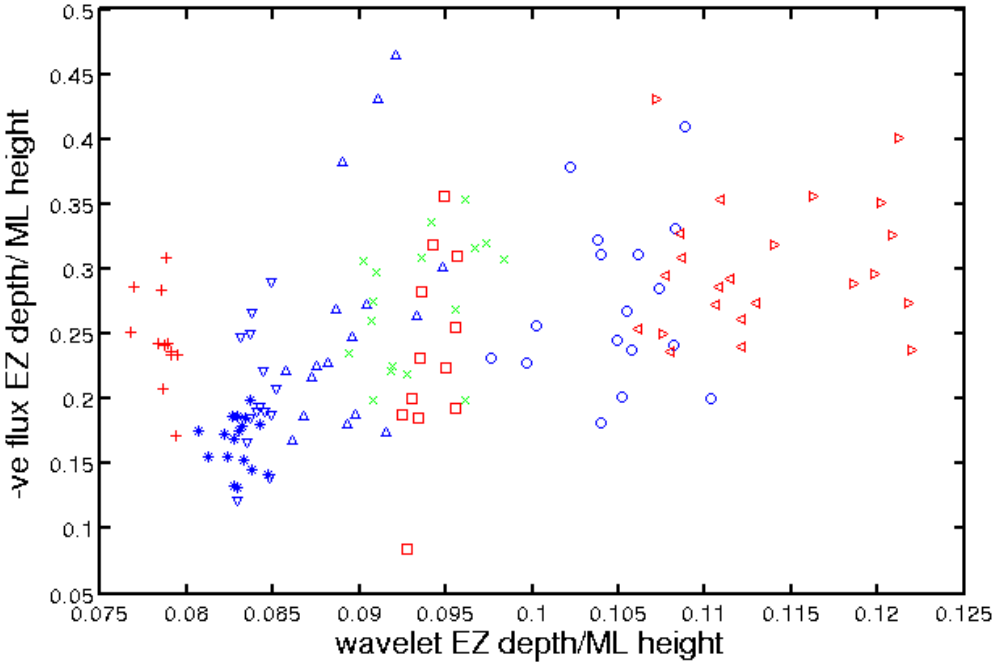

Figure 6.1. Normalised EZ depth estimated by the area of negative heat flux, plotted as a function of the normalised EZ depth estimated by the wavelet algorithm. For symbol definitions see Figure 5.2.6.

New studies of the statistics of the EZ top and bottom, made possible by the wavelet technique, have been conducted. Both a measure of the skewness and the standard deviation were found to be reliant upon the convective Richardson number. In particular the difference between the statistics of the top and bottom of the EZ were consistent with the convective Richardson number. This has given evidence for the possibility of estimating the convective Richardson number from lidar backscatter profiles of the atmosphere. Further research into the strong correlation found between the difference of the standard deviations for the EZ top and bottom and Ri_* is required. From knowing the convective Richardson number of the PBL it should then be possible to calculate the

entrainment velocity, however, there is still much uncertainty over the exact nature of the entrainment velocities relationship with the convective Richardson number. For the range of conditions used in this study the variability of the entrainment velocity does not appear to be purely a function of Ri_* but also the strength of the temperature inversion.

7. REFERENCES

Angevine, W. M., 2006: Entrainment Parameterization based on Entrainment Zone Richardson Number. *Proceedings of the 17th Symposium on boundary Layer and Turbulence, San Diego, May 22-25 2006, AMS*.

Betts, A. K., 1976: Modelling Subcloud Layer Structure and Interaction with a Shallow Cumulus Layer. *J. Atmos. Sci.,* **33**, 2363-2382.

Boers, R., E. W. Eloranta, 1986: Lidar Measurements of the Atmospheric Entrainment Zone and the Potential Temperature Jump across the Top of the Mixed Layer. *Bound.-Layer Meteorol.*, **34**, 357-375.

Boers, R. A., 1989: A Parameterization of the Depth of the Entrainment Zone. *J. Appl. Meteorol.,* **28**, 107-111.

Bretherton, C. S., 1999: An intercomparison of radiatively-driven entrainment and turbulence in a smoke cloud, as simulated by different numerical models. *Quart. J. Roy. Meteor. Soc.,* **125,** 391–424.

Brooks, I. M., 2003: Finding Boundary Layer Top: Application of a Wavelet Covariance Transform to Lidar Backscatter Profiles. *J. Atmos. Ocean. Tech.*, **20**, 1092-1105.

Davis, K. J., D. H. Lenschow, S. P. Oncley, C. Kiemle, G. Ehret, A. Giez, J. Mann, 1997: Role of entrainment in surface-atmosphere interactions over the boreal forest. *J. Geophys. Res.,* **120**, 29219-29230.

Davis, K. J., N. Gamage, C. R. Hagelberg, C. Kiemle, D. H. Lenschow, P. P. Sullivan, 2000: An Objective Method for Deriving Atmospheric Structure from Airborne Lidar Observations. J. *Atmos. Oceanic. Technol.*, **17**, 1455-1468.

Deardorff, J. W., 1974a: Three dimensional Numerical Study of the Height and Mean Structure of a Heated Planetary Boundary Layer. *Bound.-Layer Meteorol.*, **7**, 81-106.

Deardorff, J. W., 1974b: Three dimensional Numerical Study of the Turbulence in an Entraining Mixed Layer. *Bound.-Layer Meteorol.*, **7**, 199-226.

Deardorff, J. W., G. E. Willis, and B. H. Stockton, 1980: Laboratory studies of the entrainment zone of a convectively mixed layer. *J. Fluid Mech.*, **100**, 41-46.

Deardorff, J. W., 1983: Multi-limit mixed-layer Entrainment Formulation. *J. Phys. Oceanogr.*, **13**, 988-1002.

Faloona, I., D. H. Lenshow, T. Campos, Sevens, M. Van Zanten, B. Blomquist, D. Thornton, A. Bandy, and H. Gerber, 2005: Observations of Entrainment in Eastern Pacific Marine Stratocumulus Using Three Conserved Scalars. *J. Atmos. Sci.*, **62**, 3268-3285.

Gryning, S. E., A. A. M. Holtslag, J. Irwin, and B. Sivertsen. 1987: Applied Dispersion Modelling Based on Meteorological Scaling Parameters. *Atmos. Enviro.*, **21**, 79-89.

Gryning, S.-E., E. Batchvarova, 1994: Parameterization of the depth of the entrainment zone above the daytime mixed layer. *Quart. J. Royal Meteorol.* Soc., **120**, 47-58.

Kit, E. L. G., E. J. Strang, and H. J. S. Fernando, 1997: Measurements of Turbulence Near Shear-Free Density Interfaces. *J. Fluid Mech.*, **334**, 293-314.

Lenshow, D. H., P. B. Krummel, and S. T. Siems, 1999: Measuring Entrainment, Divergence, and Vorticity on the Mesoscale from Aircraft. *J. Atmos. Oceanic Technol.*, **16**, 1384-1400.

Lewellen, D. G., and W. S. Lewellen, 1998: Large Eddy Entrainment. *J. Atmos. Sci.,* **55**, 2645-2665.

Lock, A. P., M. K. Macvean, 1999a: The Parameterization of Entrainment Driven by Surface Heating and Cloud-Top Cooling. *Q. J. R. Meteorol. Soc.*, **125**, 271-299.

Lock, A. P., M. K. Macvean, 1999b: The Generation of Turbulence and Entrainment by Surface Buoyancy Reversal. Q. *J. R. Meteorol. Soc.*, **125**, 1017-1-38.

Lilly, D. K., 2002: Entrainment into Mixed Layers. Part I: Sharp-Edged and Smoothed Tops. *J. Atmos. Sci.*, **59**, 3340-3352.

Moeng, C.-H., and P. P. Sullivan, 1994: A comparison of Shear and Buoyancy Driven Planetary-Boundary-Layer Flows. *J. Atmos. Sci.*, **51**, 999-1022.

Nelson, E., R. Stull, E. Eloranta, 1989: A Prognostic Relationship for Entrainment Zone Thickness. *J. Appl. Metoerol.*, **28**, 885-903.

Perera, M. J. A. M., H. J. S. Fernando, and D. L. Boyer, 1994: Turbulent Mixing at the Inversion Layer. *J. Fluid Mech.*, **267**, 275-298.

Stevens, D. E., J. B. Bell, A. S. Almgren, V. E. Beckner, and C. A. Rendleman, 2000: Small-Scale Processes and Entrainment in a Stratocumulus Marine Boundary Layer. *J. Atmos. Sci.*, **57**, 567-581.

Stull, R. B., 1973: Inversion Rise Model based on Penetrative Convection. *J. Atmos. Sci.,* **30**, 1092-1099.

Stull, R. B., 1988: An Introduction to Boundary Layer Meteorology. Kluwer *Acad. Publ., Dodrecht-Boston-London*, 666 pp.

Sullivan, P. P., C.-H. Moeng, B. Stevens, D. H. Lenshow and S. D. Mayor, 1998: Structure of the Entrainment Zone Capping the Convective Boundary Layer. *J. Atmos. Sci,.* **55**, 3042-3064.

Tennekes, H., A. G. M. Driedonks, 1981: Basic Entrainment Equations for the Atmospheric Boundary Layer. *Boundary Layer Meteorol.*, **20**, 515-531.

Zeman, O., H. Tennekes, 1977: Parameterization of the Turbulent Energy Budget at the Top of the Daytime Atmospheric Boundary Layer. *J. Atmos. Sci.*, **34**, 111-123.

Part 2

TABLES

Table 1: Properties of simulation

Run	SHF Wm^{-2})	IS (K)	$\overline{w^*}$ (ms^{-1})	$\overline{z_i}$ (m)	$\overline{Ri}$	$\overline{w_e} \times 10^{-3}$ (ms^{-1})	Notes
IS1-SHF10	10	1	0.61	714	46.5	6.93	
IS1-SHF20	20	1	0.79	742	27.3	6.93	
IS1-SHF35	35	1	0.98	797	19.2	14.0	
IS1-SHF59	50	1	1.14	852	15.4	20.6	
IS2-SHF20	20	2	0.77	715	57.6	3.17	
Low vertical resolution	20	2		741	111	3.90	Run 7 with halved vertical resolution around the inversion
High horizontal resolution	20	2		725		3.40	Run 7 with doubled horizontal resolution around the inversion
High vertical resolution	20	2		706		2.73	Run 7 with doubled vertical resolution around the inversion
IS2-SHF30	30	2	0.90	744	39.7	5.72	
IS2-SHF40	40	2	1.01	769	30.3	8.60	
Shallow PBL	40	2	0.88	487	13.6	18.7	Same as run 8 with initial ML height reduced from 650m to 300m
IS2-SHF60	60	2	1.19	825	20.6	15.2	
-	60	2					2D runs of run 9 at a frequent output
IS2-SHF80	80	2	1.35	890	15.5	23.2	
IS4-SHF80	80	4	1.27	781	34.4	9.92	
IS10-SHF200	200	10	1.66	721	59.5	3.78	

Part 3

APPENDIXES

Appendix A: Abbreviations

$(\overline{w'\theta'})_{\min}$	Heat Flux at inversion	
$(\overline{w'\theta'})_s$	SHF	Surface heat flux
$\overline{\theta}$	Mean potential temperature within the PBL	
$\overline{w'w'}$	Vertical wind flux	
$\hat{\theta}$	Mean potential temperature in the inversion zone	
d	Thermal overshoot distance	
EZ	Entrainment Zone	
FA	Free Atmosphere	
g	gravity	
LCL	Lifting Condensation Level	
LEM	Large Eddy Model	
LES	Large Eddy Simulation	
ML	Mixed Layer	
PBL	Planetary Boundary Layer	
q	Water mixing ratio (kg/kg)	
Ri_*	Convective Richardson number	$\underline{\Delta\theta}$
Ri_g	Gradient Richardson number	
Ri_l	Local Richardson number	$N_i^2 L_H^2 / u_H^2$
S	Skewness	
t	time	
TKE	Turbulent Kinetic Energy	
w_*	Convection velocity	$\left[\frac{g z_i}{\overline{\theta}}\left(\overline{w'\theta'}\right)_s\right]^{1/3}$
w_e	Entrainment velocity	$\frac{\partial z_i}{\partial t} - w_L$
w_L	Large-scale mean vertical velocity	
z_i	Height of planetary boundary layer	
Δh	Entrainment Zone depth	
$\Delta h_{5\text{-}95}$	EZ depth estimated by the 5-95% limits of the probability distribution of the maximum gradient seen in a conserved scalar quantity	

Δh_{flux}	EZ depth estimated by the horizontally averaged area of negative buoyancy flux	
Δh_{sig_grad}	EZ depth estimated by the area of significant gradient of a horizontally area averaged conserved scalar quantity	
$\Delta h_{wavelet}$	EZ depth estimated by the wavelet analysis of a conserved scalar quantity	
$\Delta\theta$	IS	Inversion Strength
θ_*	Mixed layer temperature scale	$\dfrac{\overline{w'\theta'}_s}{\left(\dfrac{gz_i}{\overline{\theta}}\overline{w'\theta'}_s\right)^{1/3}}$
σ	Standard deviation	

Appendix B: Sensitivity Tests

In order to study the sensitivity of the entrainment results seen in this study to the resolution of the spatial grid used at the inversion, sensitivity tests have been carried out on run 7. This run had an initial inversion strength of a 2K jump across the inversion, and a surface heat flux of 20 W/m^2. These initial forcings simulate a PBL with a high Richardson number and hence represent a very stable PBL with a shallow EZ. This means that too low a resolution would have more of an affect than for a simulation of a PBL with a deeper EZ in a more turbulent environment.

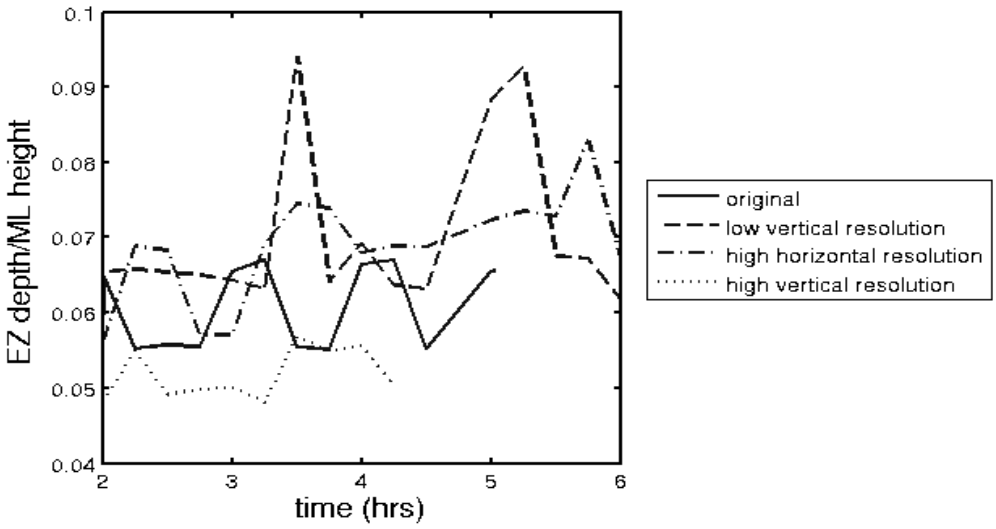

Figure B.1. The normalised EZ depth plotted as a function of time for different spatial resolutions.

The original resolution of 50m×50m×12.5m has been compared to a low vertical resolution of 50m×50m×25m, a high horizontal resolution of 25m×25m×12.5m and a high vertical resolution of 50m×50m×7m around the inversion. The effect of these varying resolutions on the EZ depth, Figure B.1., entrainment velocity, Figure B.2., magnitude of maximum negative buoyancy flux, Figure B.3., Total TKE, Figure B.4. and finally the power spectra of potential temperature, Figure B.5., have been computed.

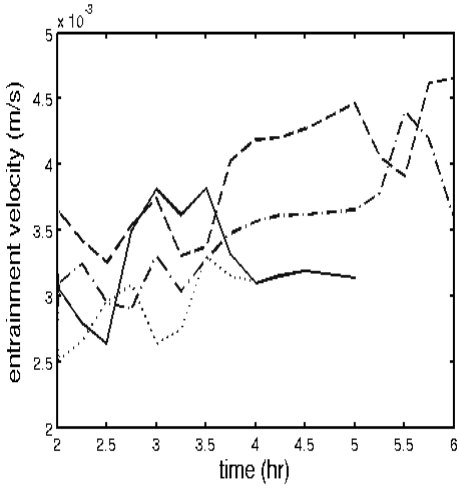

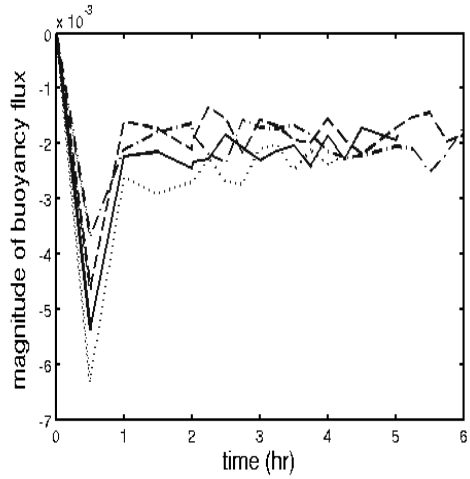

Figure B.2. (left) Entrainment velocity plotted as a function of time. Line types are defined as in Figure B.1. **Figure B.3**. (right) Magnitude of maximum negative buoyancy flux plotted as a function of time. Line types are defined as in Figure B.1.

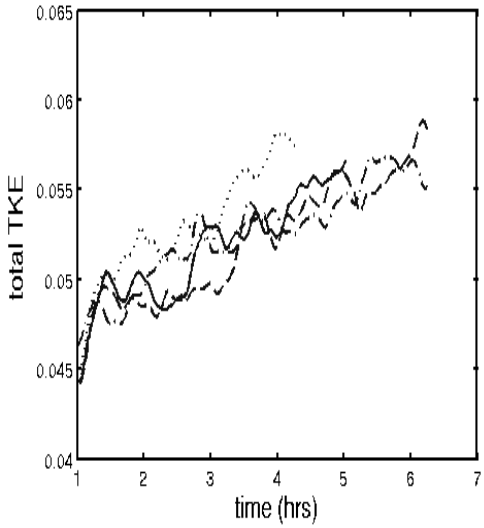

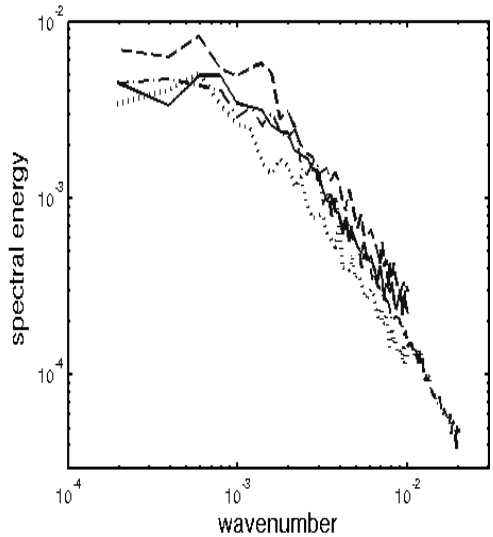

Figure B.4. (left) Total TKE plotted as a function of time. Line types defined as in Figure B.1. **Figure B.5**. (right) Sensitivity of power spectra of potential temperature to the special resolution of the inversion zone. Line types are defined as in Figure B.1.

It can be concluded that increasing the horizontal resolution will have little affect on any results seen. A decrease in the vertical resolution, although it would save time, would have too large an effect on the estimation of EZ depth so may skew results when the PBL is very stable and the EZ is small compared to the vertical resolution used. Increasing the vertical resolution also had a notable affect on the estimation of the EZ depth and entrainment velocity, predicting slightly lower values. This resolution also gave a lower estimate of the magnitude of the buoyancy flux (Figure B.3.) suggesting weaker overshooting and predicted slightly higher TKE (Figure B.4.) but the same rate of increase and the spectral energy (Figure B.5) although slightly smaller for all wave numbers had the same shape and peaked at the same value. However due to time constraints these were not seen significant enough to impose on the runs used. Nevertheless, further studies should look more into the affects of vertical resolution at the EZ, following on from the work of Stevens et al. (2000).

It is difficult to know exactly which length scales are important for accurately simulating entrainment (Stevens et al., 2000). (Lock and MacVean 1999) suggested entrainment is principally a function of the net source of kinetic energy, another scale identified by Bretherton et al. (1999) and Stevens and Bretherton (1999) is the undulation length scale, $\delta z_u = z_i/Ri$. This length scale is an approximation of the distance it takes a buoyancy force representative of the inversion strength to slow an air parcel from w_*, its updraft speed, to zero. However, this is still in much discussion.

Appendix C: The Shallow Mixed Layer

Throughout the day the PBL will grow as the surface is heated, so the depth of the PBL is a function of time. Tests have been conducted to study the affect of simulating a shallower boundary layer, typical of early morning. This time the initial setup used in run 8 was repeated but reducing the PBL depth from 600m to 350m. Run 8 and now run 8i (see table 1) both have an initial inversion strength of 2K and a surface heat flux of 40W/m^2. The affect of reducing the initial PBL depth on the potential temperature profile at 2 hours and 5 hours into the run can be seen in Figure C.1. It is clear that the altitude of the temperature inversion increases at a much fast rate for a shallower PBL and also the strength of the temperature inversion decreases much faster with time. This is because the same amount of energy is being supplied to a much smaller volume, so entrainment can happen at a faster rate which controls the growth of the PBL. A more rapidly entraining PBL will also cause the EZ to increase in depth faster and hence decrease the strength of the temperature inversion.

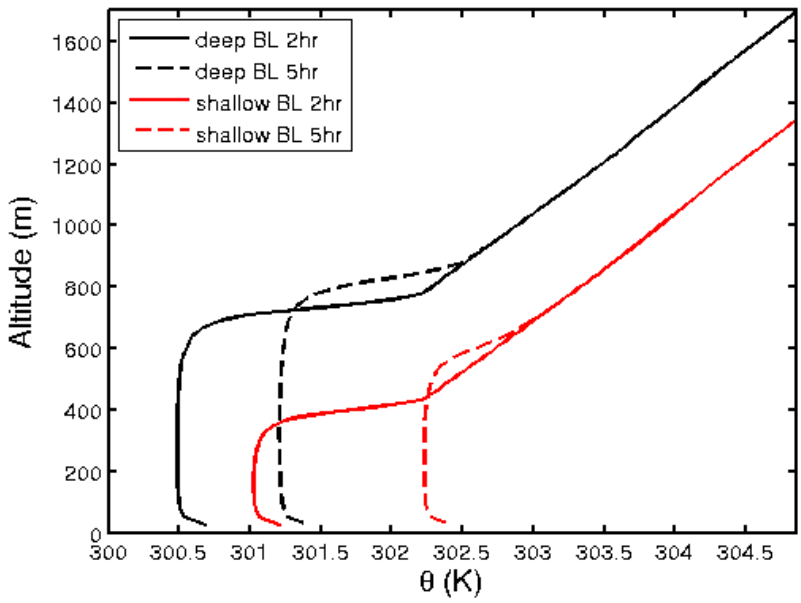

Figure C.1. Comparison of the horizontally area averaged potential temperature profiles of an initial shallow (350m) and deep (600m) BL at 2hrs and 5hrs into the model run.

From observations of the potential temperature profiles it is apparent that the shallower BL will be much more turbulent. This is confirmed in Figure C.2. where the Richardson number for the shallow and deep PBLs are compared. The Richardson number for the shallow BL layer is very low and for the first four hours has very similar values as those

seen for IS2-SHF80. However, the decrease in values occurs at a much faster rate until 5hours 15minutes in to the run where it reaches a minimum of approximately 10 and then steadily begins to rise again, which is not a pattern observed for any of the runs with the initial deep PBL (see Figure 4.1.1). This may suggest that the turbulent eddies are being constrained by the depth of the PBL (Gryning, 1987). At a similar time the rapidly increasing entrainment velocity appears to begin to decrease as well (figure C.3.). This is obviously due to there not being enough turbulence to continue to drive the previously high entrainment velocities. However, the convective velocity scale or Deardorff velocity, w*, (Figure C.4.) the updraft speed in convective thermals continues to rise steadily throughout the run. Although at a much faster rate that for that of the deep PBL and does not reach the same magnitude. For a constant PBL depth the convective scale increased logarithmically with the surface heat flux and is independent of the inversion strength, but the initial PBL also has an obvious affect.

These tests have also helped to emphasise the importance of the PBL depth and hence entrainment for the dynamics of the atmosphere.

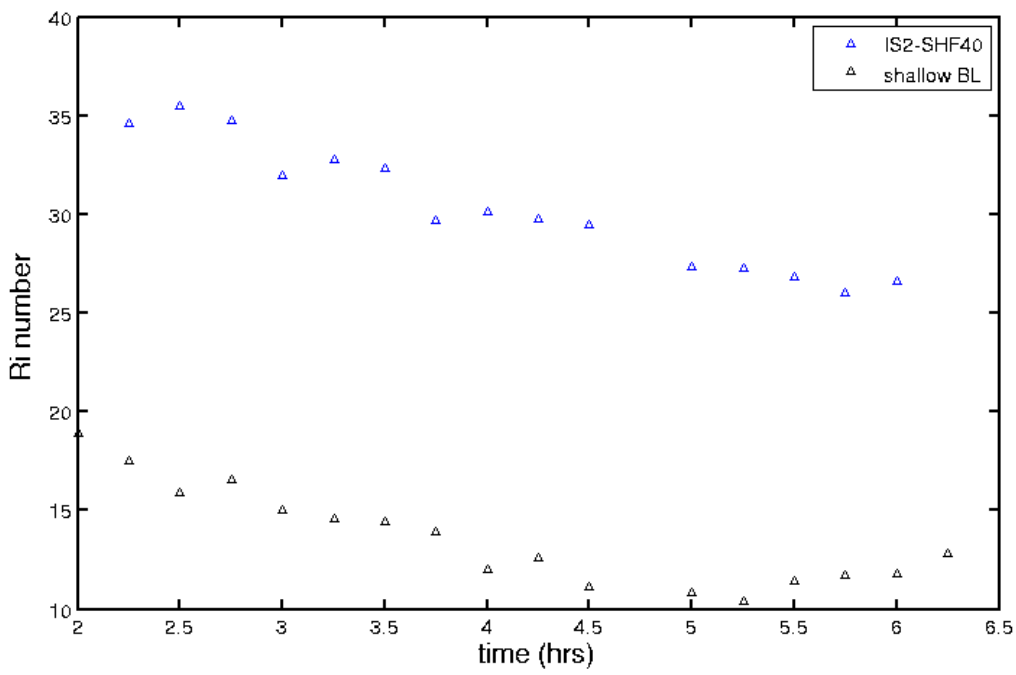

Figure C.2. Comparison of the Richardson number's progression with time for a shallow (black triangle) and deep boundary layer (blue triangle).

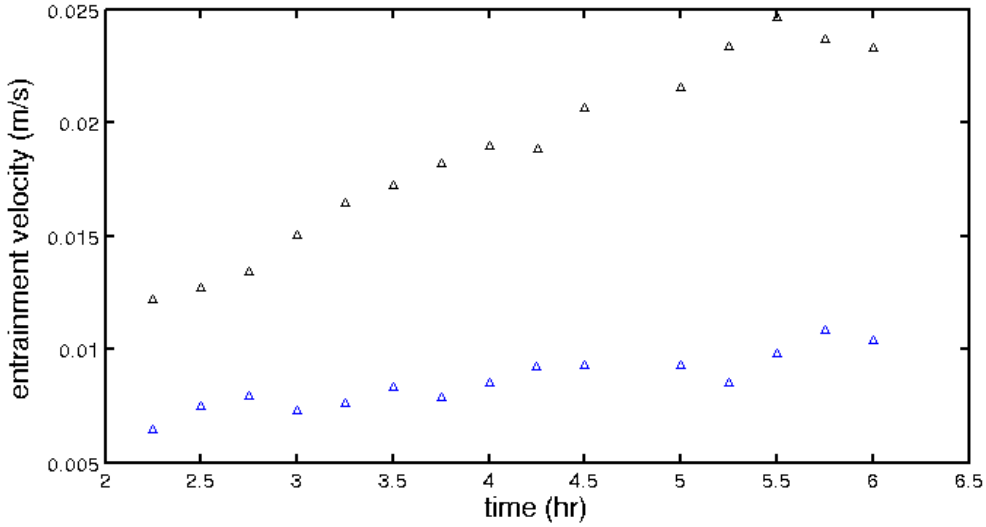

Figure C.3. Comparison of the entrainment velocity's progression with time for a shallow (black triangle) and deep boundary layer (blue triangle).

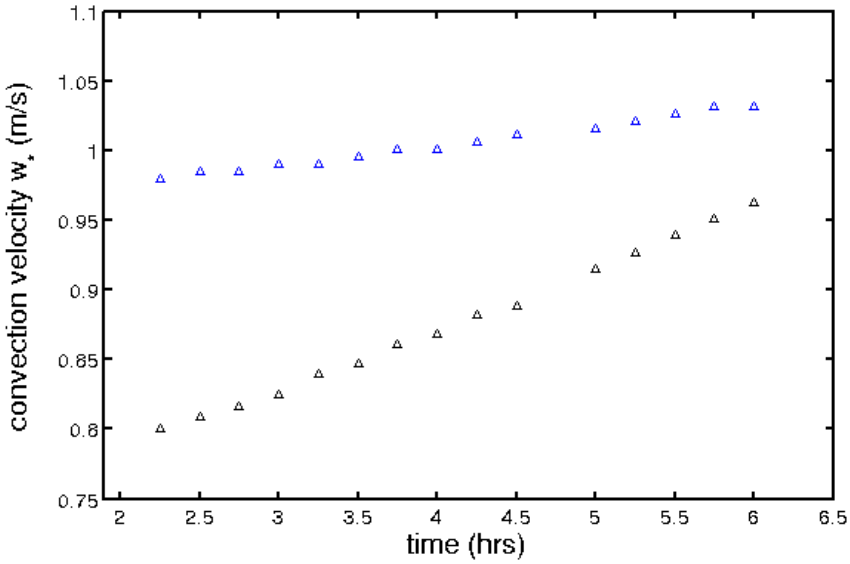

Figure C.4. Comparison of the convection velocity's progression with time for a shallow (black triangle) and deep boundary layer (blue triangle).

Running the model with a shallower PBL had no effect on any of EZ depth definitions relationship with the convective Richardson number. Figure C.5. shows how the data for the shallow PBL fits to the curve in the case of the 5-95% PBL top distribution defined EZ depth.

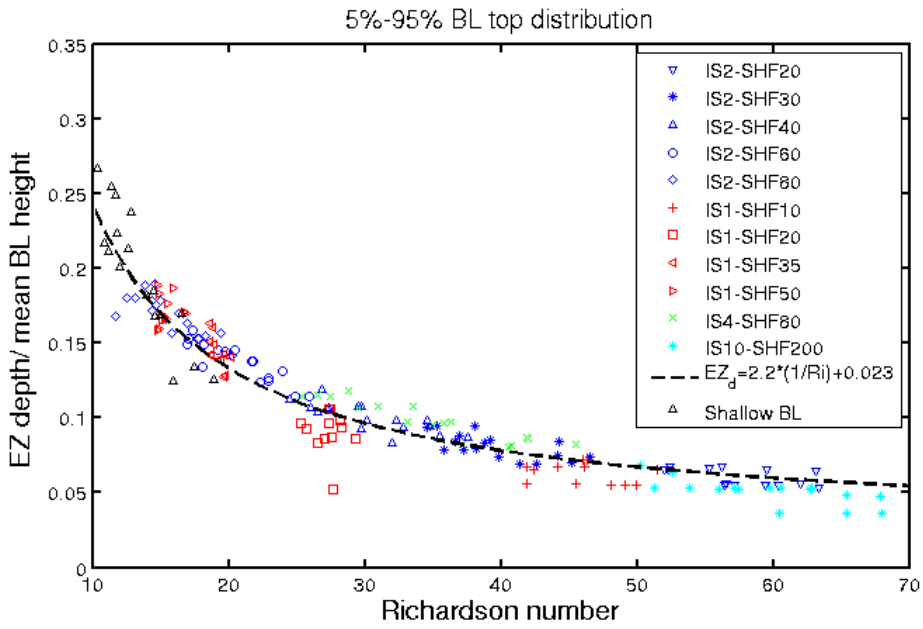

Figure C.5. An example of how the EZ depth estimated for the shallow BL is consistent with the relationship already observed.

Appendix D: Literature Review

(This is largely a repeat of my previous Literature Review, and has already been marked)

D.1. INTRODUCTION

Since the early seventies a huge effort has been made in attempting to understand the entrainment zone and its parameterization.

This paper will be looking at the history of the work that has been conducted so far in order to improve our understanding of the mechanisms involved in entrainment of the FA into the ML and how this work can be useful in the improvement of climate, forecast and pollution transport models. It will also be discussed how this work can be progressed through further studies and the limitations of what is currently possible.

D.2. PARAMETERIZATIONS

D.2.1 Definition of Boundary Layer Height

The height of the boundary between the mixed layer and the stably stratified layer is one of the defining characteristics of the entrainment zone. It is also of primary importance since it determines the volume of the atmosphere through which surface-emitted pollutants can be diluted. It is used by Sullivan et al. (1998) as a length scale to compare different boundary layers and to quantify inversion characteristics. There is no exact definition of the boundary layer height; it has been defined in four different ways:

- Flux methods

The standard flux method defines the height of the boundary layer z_{i1} as the vertical location of the averaged minimum flux

$z_{i1} = z,$ where $\langle w\theta(z)\rangle$ is minimum. (D.2.1.1)

To compute z_{i1} it is necessary to average $w\theta(x,y,z)$ in z the component and then locate the minimum flux, $\langle w\theta(z)\rangle_{\min}$. The vertical location of this minimum is then the boundary layer height z_{i1}. However, this technique ignores spatial variations in the boundary layer height and so a second method is now defined:

$z_{i2} = z$, where $[w\theta(y,z)]$ is minimum. (D.2.1.2)

this takes into account some of the spatial variability of the boundary layer height.

- Contour method

In the contour method the entrainment interface is defined by tracking the vertical location of a scalar contour, for example potential temperature contour θ_{con} in the EZ on a point-by-point basis.

$z_{i\theta} = z$, where $\theta(x,y,z) = \theta_{con}$. (D.2.1.3)

The disadvantage with this method is that it is dependent on which contour is chosen. Also the temperature contours evolve with time so this method does not represent the entrainment dynamics.

- Gradient method

The gradient method defines the boundary layer height z_{ig}, as the vertical location of the largest increase in potential temperature

$z_{ig}(x,y) = z$, where $\frac{\partial\theta(x,y,z)}{\partial z}$ is maximum. (D.2.1.4)

This method is advantageous over the contour method in that the local spatial variances of the boundary layer height are preserved and this method also follows the evolution of the interface with time. This method is favoured by Sullivan et al. (1998).

Comparison of methods: The standard flux method has large fluctuations in area and generally predicts smaller values than that of the contour or gradient method. The modified flux method gives a smoother profile as gives a line of best fit to the standard flux method as expected. The gradient and contour methods also give smooth results as they are local methods and use a larger statistical sample to estimate the boundary layer height.

D.2.2 Defining the Entrainment Zone

Simple parameterizations are often based on the EZ thickness. The thickness of the EZ is typically 30% that of the mixed layer, but is capable of reaching a depth comparable to the mixed layer (Gryning and Batchvarova, 1994). One of the first efforts made to

parameterize the EZ thickness was by Betts (1976) who assumed that it would be proportional to the ML depth.

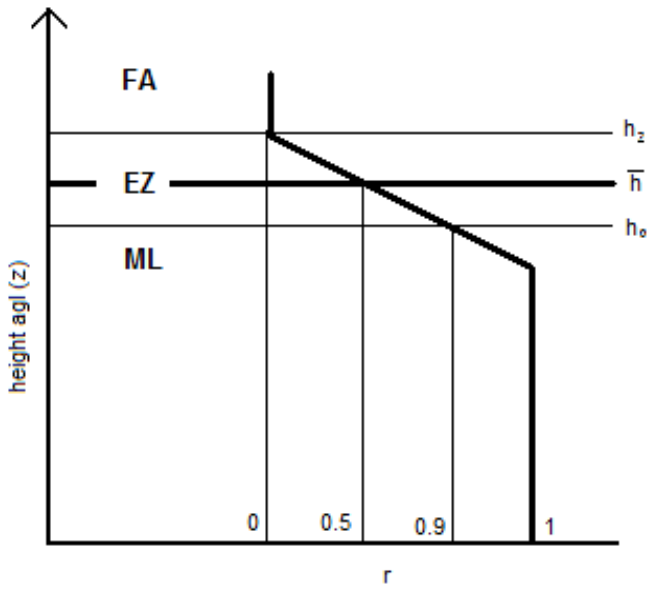

Figure D.2.2.1. Idealised vertical profile of mixing ratio (r) of mixed layer air and free atmosphere air for the case of a cloud-free convective boundary layer. FA: free atmosphere, EZ: entrainment zone, ML: mixed layer, h_2: top of EZ, $\bar{h}$:mixed-layer depth, h_o: bottom of EZ.

Since then Zeman and Tennekes (1977) have used 'parcel theory' to parameterize the EZ thickness. This relates the EZ depth to the height a rising thermal overshoots its neutral buoyancy level into the stable air above. The characteristic velocity of the rising thermals is taken to be proportional to the standard convective velocity scale obtained from bottom-up scaling. This method has shown a dependence between normalized EZ depth and a convective Richardson number. However water tank experiments by Deardorff et al. (1980) and atmospheric measurements conducted by Boers and Eloranta (1986) do not support this theory. Using an energy-balanced model, Boers (1989) improved the fit of the data in the Boers and Eloranta (1986) work by suggesting that the normalized depth of the EZ depended on the convective Richardson number to the -1/2 power, whereas Deardorff (1983) suggested the relationship to be of the -1/4 power. However, Gryning and Batchvarova (1994) define the entrainment Richardson number as

$$Ri_E = \frac{(g/T)\Delta\theta h}{w_e^2} \qquad \text{(D.2.2.1)}$$

which they used to parameterise the change in height as follows:

$$\frac{\Delta h}{h} \propto (Ri_E)^{-1/3}. \qquad \text{(D.2.2.2)}$$

Deardorff et al. (1980) defined the EZ bottom and top heights as the altitudes where the buoyancy flux vanishes and the average boundary layer height where it reaches its most negative value. They characterised the depth of the ML, $\bar{h}$ as the height at which 50% of the air has ML characteristics and the bottom of the EZ, h_0 and the top of the EZ, h_2 as the heights corresponding to air with 90% and 5% characteristics of ML air respectively. See Figures D.2.2.1 and D.2.2.2. Wilde et al. (1985) however, proposed the EZ top and bottom heights to be given the heights at which respectively 4% and 98% of the air has ML air characteristics. This is a still a major problem with this type of technique for defining the EZ depth.

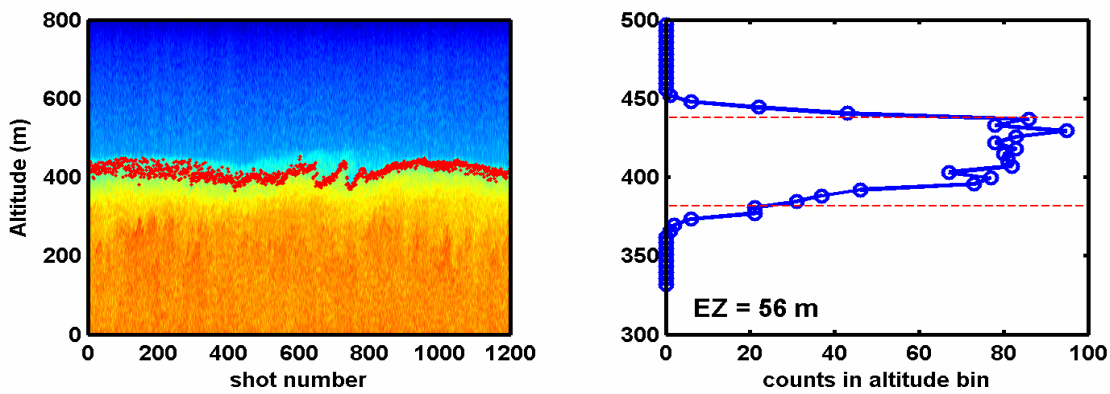

Figure D.2.2.2. (right) lidar plot of backscatter from aerosols.(left)Illustration of the definition of the entrainment zone as the interval over which the area-averaged fraction of free-troposphere air lies between some predefined limits (typically 5%-95%)

Figure D.2.2.3 shows how the EZ may also be defined as the area where some scalar quantity has a significantly higher gradient. However it can be seen by comparing the two methods used in Figures D.2.2.2 and D.2.2.3, which have both been applied to the same data that the estimated EZ depths vary widely, from 56m using the percentile method to approximately 200m using the gradient method. The difficulty with the gradient method is that it is not always clear where the area of significant gradient begins and ends.

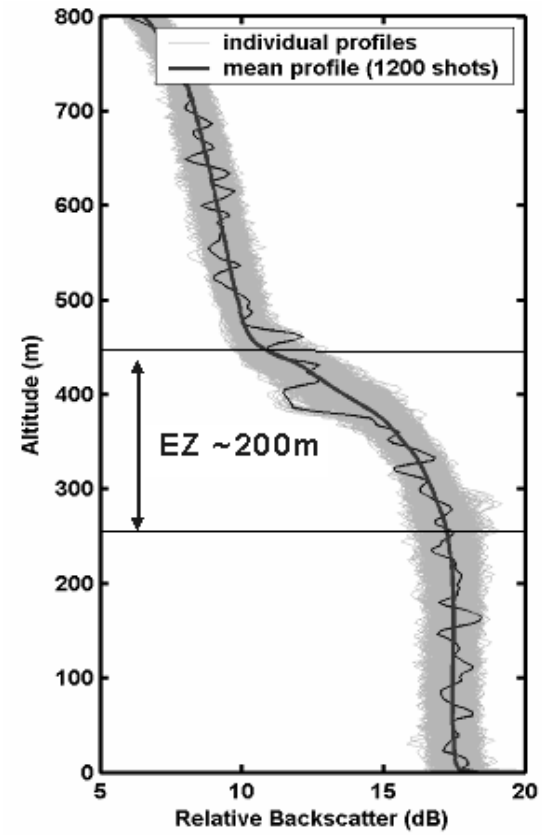

Figure D2.2.3. Definition of the entrainment zone as the vertical interval over which the mean profile of some scalar quantity (water vapour mixing ratio, aerosol concentration) has a significant gradient.

Other area averaged methods for defining the EZ include finding the area of negative heat flux, see figure D.2.2.4.

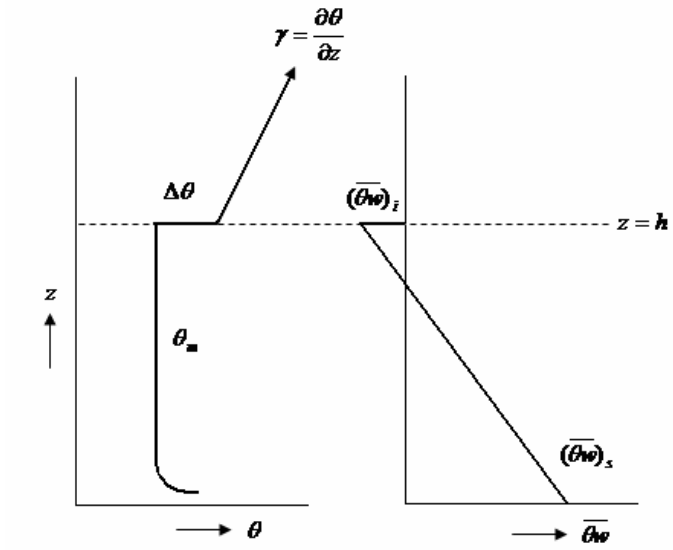

Figure D.2.2.4: The profile of potential temperature, θ,(left) and the heat flux distribution (right) with the EZ modelled as a discontinuous jump in the potential temperature.

The total heat flux decreases linearly with height from the ground to the point where $\overline{\theta w}$ is a minimum. The profile is linear in order to ensure that the boundary layer heats up uniformly.

The EZ consists of small-scale turbulent thermals embedded in large-scale fluctuations induced by gravity waves, so the use of area averaged techniques must be filtered to remove the effect of gravity waves. This introduces wavelet analysis which is an objective method to retrieve structual details from data collected from lidar. Much use, for this purpose has been made of the Haar function or step function (Davis et al. 2000; Cohn et al. 2000). This method is based on the similarity between the sharp, coherent changes in aerosol content and the step function, see figure D.2.2.5. The algorithm is applied to a single vertical lidar backscatter profile (see § D.4.2). The step or Haar function is defined as

$$h\left(\frac{z-b}{a}\right)=\begin{cases}-1:\ldots b-\frac{a}{2}\le z\le b\\ 1:\ldots b\le z\le b+\frac{a}{2}\\ o:\ldots elsewhere,\end{cases}\quad,\quad \text{(D.2.2.3)}$$

where z represents the distance in the vertical in this application, and a and b describe the dilation and translation of the function, respectively.

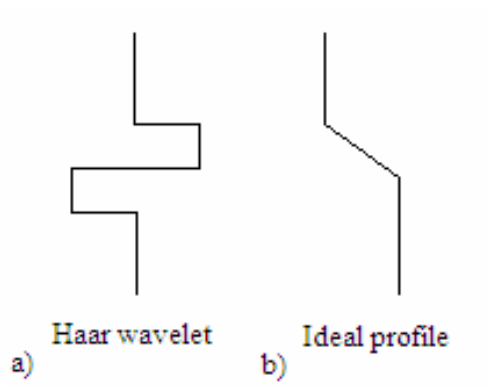

Figure D.2.2 5. a) The shape of a Haar wavelet and (b) idealised backscatter profile, with uniform backscatter in the ML, weak backscatter in the free atmosphere above and a transition through the entrainment zone.

Techniques based on $-db/dz$ are difficult to implement because they amplify noise. This results in a profile where no maximum is evident. Therefore to implement this

technique it is necessary to take an average of a succession of profiles and then to average in the vertical as well.

Cohn and Angevine (2000) made use of wavelets because of the 'relative simplicity to implement a wavelet algorithm and the ability to use the wavelet to recognise the scale of the identified feature.' This scale can also be used to test the consistency of the algorithm result. Once the algorithm has been applied it can be used to look at the EZ thickness, which is very variable with time, for example recent entrainment will make the interface large. Cohn and Angevine (2000) calculated the change in EZ depth by looking at a time distribution of the boundary layer top. The difference between specifically chosen percentiles of the height of the interface (chosen to remove any outliers) gives the change in EZ depth. They also excluded thickness measurements above 800m as these are likely to be false or from a time when the boundary layer top was ill-defined.

The technique utilising the Haar wavelet is found to be effective when the vertical gradient of the backscatter is small within and above the boundary layer, and when the inversion is sharp and well defined. However, for lidar backscatter, this is often not the case, for example under stable stratification when the inversion may be deep and not well defined, and vertical gradients are common. Brooks (2003) has developed an alternative approach using multiple wavelet dilations which can identify both the upper and lower limits of the backscatter transition zone associated with the inversion whilst insensitive to mean vertical gradients in the background signal. This enables more detailed information on the small-scale structure of the inversion and the EZ. Figures D.2.2.6 and D.2.2.7 show Brooks (2003) technique applied to lidar data. These figures show that the relative position of the top and bottom of the inversion using the technique of Brooks (2003), and estimates of depth using the method of Davis et al. (2000) do not remain constant, this emphasises the sensitivity of the estimate of a single value for the boundary layer top. The varying behaviour of the inversion limits could be used to illustrate the mixing processes related to different atmospheric conditions, to give a greater insight into the entrainment process.

Steyn et al. (1999) also made attempts to overcome problems associated with the Haar wavelet technique by utilising an approach which employs the entire backscatter profile. Steyn et al. (1999) proposed fitting an idealised backscatter profile to the observed data by minimising a measure of agreement between the two profiles. This type of method,

however, can only detect a ML with structures that match that particular ideal. So could not be used in cases of clean, near-surface air overlain by aerosol laden air.

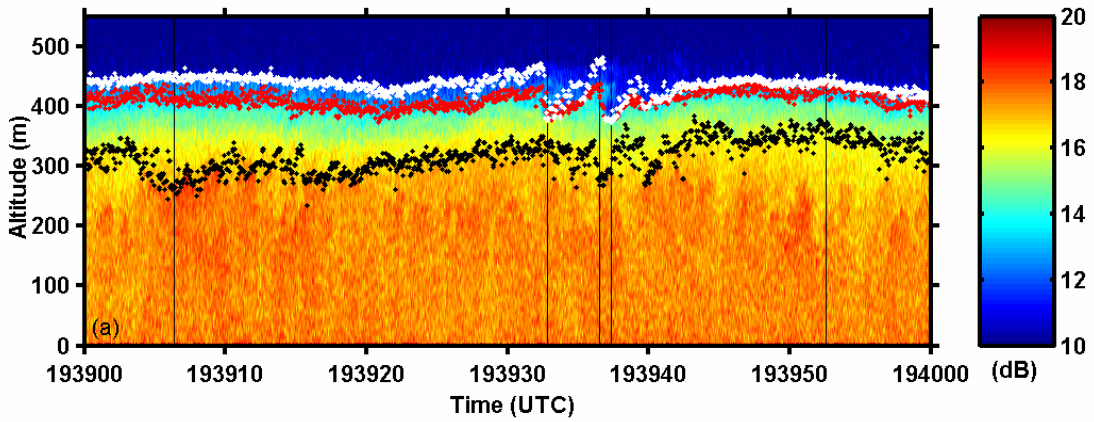

Figure D.2.2.6. Estimates of the top (white circles) and bottom (black circles) of the inversion using technique Brooks (2003), and estimates of depth (dark grey circles) using method of Davis et al. (2000)

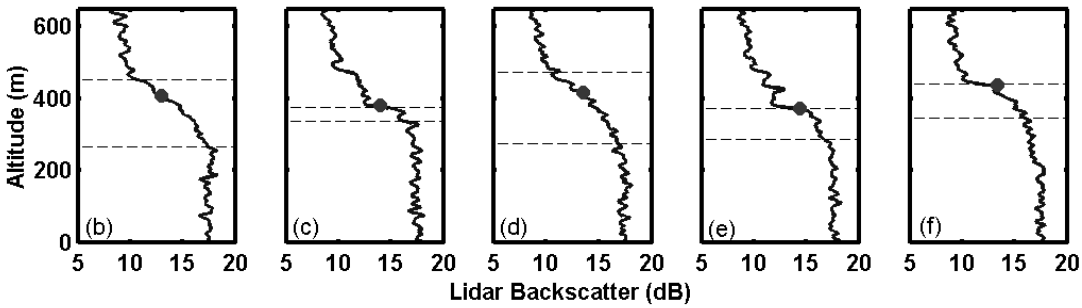

Figure D.2.2.7. Lidar backscatter profiles at the locations indicated by the vertical lines in Figure D.2.2.6. Dashed lines indicate the upper and lower limits of the inversion identified by Brooks (2003). Dots indicate the boundary layer top estimated using the approach of Davis et al. (2000).

D.2.3 Parameterization of the Energy Budget

In order to write simplified equations for momentum and heat of entrainment in the atmosphere Tennekes and Driedonks (1981) assumed that turbulence inside the boundary layer was strong enough to maintain a uniform distributions of wind direction, wind speed, and potential temperature in the vertical direction, limiting to daytime conditions as during the night turbulence hardly ever is strong enough for these assumptions. They also took the surface layer to be comparatively thin to the boundary

layer and the inversion which caps the boundary layer to be infinitesimally thin. Using these assumptions they came up with these relations for the change in the temperature jump $\Delta\Theta$ across the inversion and the change in wind velocity jumps ΔU and ΔV:

$$\begin{aligned}
\frac{d}{dt}(h\Delta\Theta) &= \gamma h\frac{dh}{dt} - (\overline{\Theta w})_s, \\
\frac{d}{dt}(h\Delta U) &= S_x h\frac{dh}{dt} - (\overline{uw})_s + fh\Delta V, \\
\frac{d}{dt}(h\Delta V) &= S_y h\frac{dh}{dt} - (\overline{vw})_s - fh\Delta U.
\end{aligned} \qquad \text{(D.2.3.1)}$$

where S_x, S_y refer to the velocity gradients above the mixed layer and $\overline{\Theta w}$ is the vertical heat flux. This illustrates that the ML entrains an amount of heat proportional to $\overline{\Delta\Theta}$ times d*h* if the inversion base rises by d*h*.

Unfortunately these conservation equations do not satisfy closure conditions. In order too obtain solutions, heat and momentum surface fluxes have to be specified in terms of mixed layer variables.

The energy budget at the inversion base is (Zeman and Tennekes, 1977):

$$\left(\frac{\partial \bar{e}}{\partial t}\right)_i = \frac{g}{T}\left(\overline{\theta w}\right)_i - \frac{\partial}{\partial z}\left(\overline{ew} + \overline{pw}/\rho\right)_i - \left(\overline{uw}\right)_i \Delta U/d - \left(\overline{vw}\right)_i \Delta V/d - \varepsilon_i \qquad \text{(D.2.3.2)}$$

where ε is the energy dissipation rate, *p* is pressure and ρ is density. The main problem in representing any mechanical production terms properly for a one-layer model is that $\partial U/\partial z \to \infty$ and $\partial V/\partial z \to \infty$ at the inversion base. So it is necessary to estimate gradients for an undetermined EZ depth. This problem can be overcome by integrating the local energy budget over the entire ML or by writing an energy budget for an EZ of finite thickness (Deardorff, 1979). However Tennekes and Driedonks (1981) believe that neither of these solutions are adequate and (D.2.3.2) is preferred as it demonstrates that 'the downward buoyancy flux at the entrainment interface is not necessarily a small fraction of the local energy consumption, while the net conversion of kinetic energy into potential energy for the mixed layer as a whole is almost certainly a small fraction of the overall energy consumption by the turbulence.'

D.3. MODELS

Models used to represent the effects of turbulence in the boundary layer include simple zero order models which specify directly the boundary layer profile, first order models in which the turbulent fluxes are parameterized in terms of mean variables and second order models in which triple correlations are parameterized. These models can then be used in practice in a large-scale climate or numerical weather prediction model.

The most straight forward zero-order models of the ML growth assume the turbulence is strong enough to maintain a layer of nearly uniform potential temperature distribution, capped by the EZ which may be represented by a step-like potential-temperature jump. This assumption of a uniform distribution in the ML is in agreement with observations however the step-like jump is not. See Figure D.2.2.4. The zero-order model is particularly suited to cases where the vertical gradients are small throughout most of the boundary layer and cases where the inversion capping the boundary layer is strong. This is generally observed during periods of significant convective activity over land. In these models the ML is usually considered to be dynamically inactive and shear terms are neglected, allowing the boundary layer to be modelled as a single layer. In these models the entrainment is parameterized by the buoyancy flux ratio A_{Rv}, defined as $\left(\overline{w'\theta'_v}\right)_{\bar{h}} = -A_{Rv}\left(\overline{w'\theta'_v}\right)_s$, where s and $\bar{h}$ refer to the surface and boundary layer top respectively.

Model predictions of entrainment vary widely because of the irregular nature of the interface, the lack of data to guide model development and the small turbulent scales which may be important within the EZ. The very irregular boundary layer top is caused by early morning growth coupled with strong wind shear across the EZ.

In Gryning and Batchvarova (1994) they modelled the EZ thickness using the energy budget of eddies from the mixed-layer that penetrate the EZ, this leads to a relation between normalized EZ depth and an entrainment Richardson number that is not restricted to purely convective conditions.

D.4. DATA COLLECTION AND EXPERIMENTS

For a better understanding of the way entrainment works it is necessary to understand the way that turbulence behaves, especially how it is maintained and its structure in the

vertical direction. To gain this knowledge field experiments have been conducted collecting data via radiosondes and lidar on aircrafts (Boers et al., 1986; Flament et al., 1997; Kiemle et al., 1998; Steyn et al., 1999), and experiments have been conducted in the laboratory (Heidt, 1977; Deardorff et al., 1980) and work has also been done to simulate the large-eddy structure of the turbulence using computers (Brown, 1996; Lilly, 2002; De Roode et al., 2004).

D.4.1 Laboratory

Hiedt (1977) studied penetrative convection within an initially stably stratified fluid heated from below, in order to investigate the growth of the mixed layer and the entrainment at the boundary. The experiments were performed in a glass tank. A stable stratification was established by allowing water to flow slowly into the tank with constantly increasing temperatures. The tank was heated from below and the developing mixed layer visualised using shadowgraphs. The initial temperature gradient, heat flux, height of the mixed layer and vertical temperature profiles were simultaneously measured. The time dependent heat flux at the bottom of the tank was determined from the measured values of the flow rate of the water through the heat exchanger and the temperature difference between the inlet and the outlet.

The results were found to agree well with theoretical results conducted by Ball (1960) and Lenschow (1973), although this model was only suitable for identical or similar physical processes. In the atmosphere, however, pure windless convection is rare. Normally wind shear would be present creating turbulence near the ground. The influences of humidity and solar radiation may also be important. Similar tests were also carries out by Deardorff et al. (1980).

D.4.2 Observational

Measurements of EZ are sparse because of the altitude above ground and the great spatial and temporal variability of the interface. Horizontal and vertical structures of the boundary layer have traditionally been observed in situ by utilizing balloons, towers and aircrafts. These observations are generally continuous in time measured at a few discrete altitudes. Recent development of remote sensing techniques such as lidar, radar and sodar has made it possible to obtain nearly continuous rang-resolved observations of the atmosphere.

Field experiments were conducted by Dreidonks (1982) in 1977 and 1978, using radiosondes, in which the mixed-layer height was predicted using the entrainment formulation $-\overline{\theta w_h} = 0.2\overline{\theta w_s} + 5u_o^3 T / gh$. It was concluded that deriving the value of *h* from radiosondes profiles is subject to a statistical sampling error, due to the convective plumes distorting the local interface between turbulent and non-turbulent air. Although this error was found to be independent of choice of model and a more complex entrainment model would not have improve these results.

The EZ can be characterized by large gradients of mean quantities, for example relative humidity and aerosol content. This has been used widely in experiments using lidar (Light Detection And Ranging), which returns a profile of lidar backscatter ratio, these profiles can be used to extract EZ thickness and ML depth. See figure D.2.2.6. Lidar systems create a large volume of data and automated processing is essential to make full use of this data. Hägeli et al. (2000) study the different techniques developed to analyse lidar data. All of these determine the border between the boundary layer and the FA air as a first step and then use statistical means to determine the ML depth and then the EZ thickness. The main problem with using lidar data to determine the EZ depth is the ambiguity in determining the EZ bottom height (see §2.2 Defining the EZ). Utilising wavelet methods can help to objectively retrieve structural details from the backscatter.

Davis et al. (1997) took the EZ height to be the mean boundary layer height of the entire flight leg and used its standard deviation as a measure of the EZ thickness. This experiment used aircrafts to get in-situ measurements of direct eddy fluxes and mean measurements throughout the boundary layer and lidar backscatter profiles from flight legs above the boundary layer. These measurements were used to investigate the evolution of the convective boundary layer over the boreal forests of Saskatchewan and Manitoba. They found a link between boundary layer growth, the vertical flux divergences, the boundary layer cloud formation, with cloud activity peaking in the midday in response to rapid boundary layer growth. Davis et al. (1997) concluded that their results illustrated the 'usefulness' of an aircraft carrying both direct sensors for measuring means and fluxes of boundary layer variables and a remote range-resolving sensor.

Kiemle et al. (1998) concluded from their experiments making use of lidar measurements that this technique for determining the EZ is only feasible when the atmospheric backscattering is horizontally homogeneous and when there is a backscatter gradient across the EZ. This method is not appropriate if the aerosol

concentration is vertically homogeneous and horizontally heterogeneous as may be the case due to forest fire. It is also useless when hygroscopic aerosol growth is present in the boundary layer which would cause an extreme increase in the backscatter.

Cohn et al. (2000) observed the boundary layer height and EZ thickness using two lidars and a radar wind profiler. The wind profiler depends on the refractive index structure with in the boundary layer (moisture gradients and turbulence strength) to extract this information. Although the two mechanisms involved in these backscatter measurements are very different there was found to be good agreement between the two in calculating the boundary layer height. However, comparison of the EZ thickness showed less agreement. To analyse the lidar measurements the Haar continuous wavelet transform of the backscatter profile was used. The algorithm used could have been improved by adding in 'continuity checks to identify possible outliers and by reporting a confidence in the result based on continuity and competing features of the wavelet coefficient map'. In their results the effect of backscatter from clouds rather than aerosols was a huge uncertainty. The relationship of clouds to the EZ is largely a matter of definition and convention and can especially be a problem for moderate cloud fractions. Another uncertainty in processing lidar data was found to be the residual layer. After the afternoon collapse of the boundary layer a residual layer containing properties of the boundary layer may become detached from the actual boundary layer. Sometimes this residual layer may still be present until the next day's boundary layer grows into it. Figure D.4.2.1 demonstrates this. The wavelet algorithm may recognise the upper boundary of this residual layer as the boundary layer top because it represents a decrease in back scatter. A simple way of eliminating this problem used by Cohn et al. (2000) is to limit the altitude range for the boundary layer top.

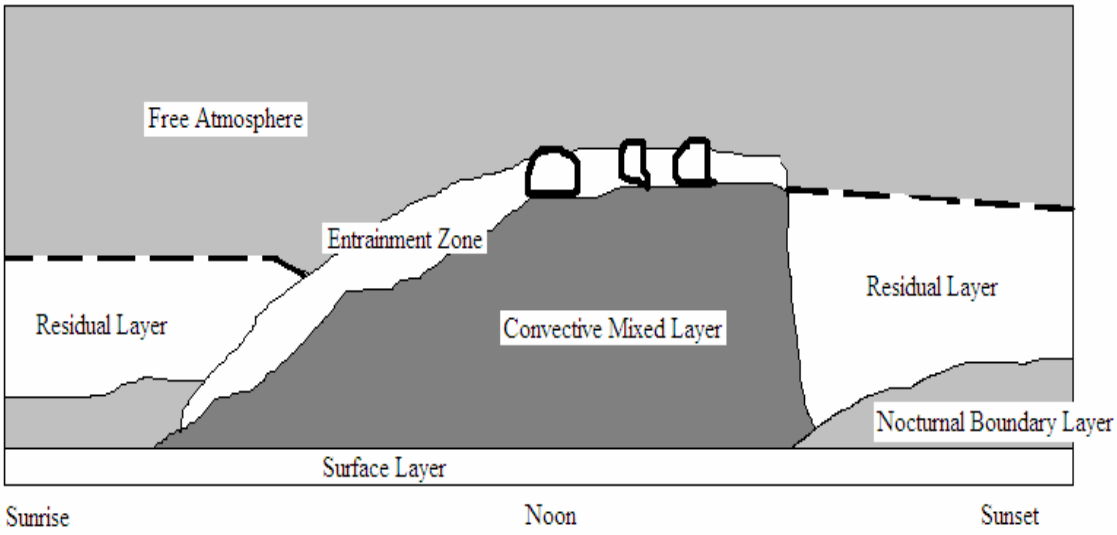

Figure D.4.2.1. A sketch of typical boundary layer evolution (Cohn et al. 2000)

D.4.3 Simulations

Entrainment in simulated models may come from several sources. Preferably the model would be able to simulate the actual physical processes which lead to entrainment, such as overturning of material surfaces pulling air from the stratified FA into the ML or vortical structures in the boundary layer scouring material of the base of the inversion.

Stevens et al. (2000) made use of a large eddy simulation (LES) model to investigate entrainment in a marine boundary layer. They were particularly looking at the effect of varying the resolution of the simulations. They discovered that the thickness of the inversion, the depth of entraining eddies, and the shape of vertical velocity spectra were determined mainly by the chosen mesh spacing of the model. A common problem associated with the simulation of entrainment is a lack of high resolution at the inversion. Sullivan et al. (1996) added grid nesting capability to the LES code making it possible to refine the grid in a selected region of the computational domain, particularly the inversion once it has been located.

Stevens et al. (2000) experiment involved simulating a turbulent boundary layer underneath a strongly stratified inversion, to isolate the effect of long-wave radiative cooling on entrainment by removing the moisture effects on buoyancy. As they wished to include clouds in their model they needed to include the additional source of turbulence from evaporative cooling caused by the mixing of saturated boundary layer air at the cloud top with unsaturated above inversion air.

The LES model was also been used by Sullivan et al. (1998) in which it was shown the entrainment mechanics were closely linked the Richardson number. At low Richardson number, the rotational motions are strong enough to fold the interface and draw in warmer inversion fluid to the plume's edge, resulting in entrainment. For a higher Richardson number the strong stability of the inversion prevents large-scale folding of the inversion interface, and instead strong horizontal downward motions near the plume's edge pull down pockets of warm air below the inversion height, which are then entrained into the ML due to turbulence.

D.5. FUTURE WORK

As computers become ever more powerful and with the difficulties and costs involved with laboratory and field experiments, large eddy simulations are becoming more dominant in evaluation of parameterization methods, these studies need to look at both equilibrium and time dependent problems. Such experiments need to be validated by observations from the atmosphere and sensitivity to parameterizations and resolution need to be checked. Using these experiments further field work and data analysis are required to relate the remotely sensed variables to in situ measurements.

It has also be noted in Dreidonks' (1982) work that further study on how humidity will effect the ML growth needs to be conducted especially because of its association with the prediction of the formation of clouds at the top of the ML. Cohn et al. (2000) suggested further work is needed to remove outliers from airborne air measurements, to identify layers such as residual layers and to properly analyze profiles that contain clouds.

Work conducted by myself during next year will be utilizing large eddy simulations to study the entrainment mechanisms and try to alleviate some of these current problems. The parameterization of the EZ by mixed layer properties will be looked at in detail which may then be used to analyse in-situ data. I will also be looking at possible correlations in definitions of the EZ thickness used so far, to try to determine an unambiguous definition for the EZ thickness. Studies of Brooks (2003) wavelet covariance transform will also be conducted to look at finding the boundary layer top to be related back to in-situ measurements. I shall also be exploring the relationship between the entrainment rate and the inversion and entrainment zone structure.

D.6. FURTHER REFERENCES

Ball, F. K., 1960: Control of Inversion Height by Surface Heating. *Quart. J. Roy. Meteorol. Soc.*, **86**, 483-494.

Batchvarova, E., S.-E. Gryning, 1994: An Applied Model for the Height of the Daytime Mixed Layer and the Entrainment Zone. *Bound.-Layer Meteorol.*, **71**, 311-323.

Brown, A. R., 1996: Evaluation of Parameterization schemes for the Convective Boundary Layer using Large-Eddy Simulations Results. *Bound.-Layer Meteorol.*, **81**, 167-200.

Cohn, S. A., W. A. Angevine, 1999: Boundary Layer Height and Entrainment Zone Thickness Measured by Lidars and Wind-Profiling Radars. *J. Applied Phys.*, **39**, 1233-1247.

Deardorff, J. W., 1979: Prediction of Convective Mixed-Layer Entrainment for Realistic Capping Inversion Structure. *J. Atmos. Sci.*, **36**, 424-436.

De Roode, S. R., H. J. J. Jonker, P. G. Duynkerke, B. Stevens, 2004: Countergradient Fluxes of conserved Variables in the clear Convective and Stratocumulus-Topped Boundary Layer: the Role of the Entrainment Flux. *Bound.-Layer Meteorol.*, **112**, 179-196.

Driedonks, A. G. M., 1982: Models and Observations of the Growth of the Atmospheric Boundary Layer. *Bound.-Layer Meteorol.*, **23**, 283-306.

Driedonks, A. G. M., H. Tennekes, 1984: Entrainment Effects in the Well-Mixed Boundary Layer. *Bound.-Layer Meteorol.*, **30**, 75-105.

Flament, C., J. Pelon, P. H. Flament, P. Durand, 1997: Lidar Determination of the Entrainment Zone Thickness at the Top of the Unstable Marine Atmospheric Boundary Layer. *Bound.-Layer Meteorol.*, **83**, 247-284.

Flament, C., J. Pelon, B. Brashers, R. A. Brown, 1999: Evidence of a Mixed-Layer Dynamics Contribution to the Entrainment Process. *Bound.-Layer Meteorol.*, **93**, 47-73.

Hägeli, P., D. G. Steyn, and K. B. Strawbridge, 2000: Spatial and Temporal Variability of Mixed-Layer Depth and Entrainment Zone Thickness. *Bound.-Layer Meteorol.*, **97**, 47-71.

Heidt, F. D., 1977: the Growth of the Mixed Layer in a Stratified Fluid due to Penetrative Convection. *Bound.-Layer Meteorol.*, **12**, 439-461.

Kiemle, C., G. Ehret, 1998: Airborne Lidar Studies of the Entrainment Zone. *Proceedings 19th International Conf. on Laser Radar, Annapolis*, pp395-398.

Lenschow, D. H., 1973: Two Examples of Planetary Boundary Layer Modification over the Great Lakes. *J. Atmos. Sci.*, **30**, 568-581.

Stage, S. A., J. A. Businger, 1981: A model for Entrainment into Cloud-Topped Marine Boundary Layer. Parts I & II. *J. Atmos. Sci.*, **38**, 2213-2242.

Stevens, D. E., and C. S. Bretherton, 1997: A forward-in-time advection scheme and adaptive multilevel flow solver for nearly incompressible atmospheric flow. *J. Comput. Phys.,* **129,** 284–295.

Steyn, D. G., M. Baldi, R. M. Hoff, 1999: The Detection of Mixed Layer Depth and Entrainment Zone Thickness from Lidar Backscatter Profiles. *J. Atmos.Ocean. Tech.*, **16**, 953-959.

Sullivan, P. P., J. C. McWilliams, C.-H. Moeng, 1996: A Grid Nesting Method for Large-Eddy Simulation of Planetary Boundary-Layer Flows. *Bound.-Layer Meteorol.*, **80**, 167-202.

vanZanten, M. C., P. G. Duynkerke, J. W. M. Cuijpers, 1999: Entrainment Parameterization in Convective Boundary Layers. *J. Atmos. Sci.,* **56**, 813-828.

Wilde, N. P., R. B. Stull, E. W. Eloranta, 1985: The LCL Zone and Cumulus Onset. *J. Clim. Appl. Meteorol.*, **24**, 640-657.